T2R2 東京科学大学 リサーチリポジトリ
Science Tokyo Research Repository

論文 / 著書情報
Article / Book Information

題目(和文)	
Title(English)	Ball-milled Indonesian natural bentonite application for manganese removal on acid mine drainage: batch and column study
著者(和文)	PrastisthoWidyawanto
Author(English)	Widyawanto Prastistho
出典(和文)	学位:博士(工学), 学位授与機関:東京工業大学, 報告番号:甲第11016号, 授与年月日:2018年12月31日, 学位の種別:課程博士, 審査員:日野出 洋文,MARIQUIT EDEN GAN,江頭 竜一,高橋 史武,竹村 次朗,KURNIAWAN WINARTO
Citation(English)	Degree:Doctor (Engineering), Conferring organization: Tokyo Institute of Technology, Report number:甲第11016号, Conferred date:2018/12/31, Degree Type:Course doctor, Examiner:,,,,,
学位種別(和文)	博士論文
Type(English)	Doctoral Thesis

Powered by T2R2 (Science Tokyo Research Repository)

Ball-milled Indonesian natural bentonite application for manganese removal on acid mine drainage: batch and column study

A dissertation submitted to

TOKYO INSTITUTE OF TECHNOLOGY

for the degree of

DOCTOR OF ENGINEERING

by

Widyawanto Prastistho

Department of International Development Engineering

Graduate School of Science and Engineering

Tokyo Institute of Technology

November 2018

List of Content

List of Figure

List of Table

CHAPTER 1
Introduction

This chapter provides brief explanation about: acid mine drainage (AMD) and its environmental impact; bentonite review, its challenge to optimize the modification using milling technique, and the potential as AMD remediation material; batch and column sorption test review. Objectives and research limitation are presented in the last section of this chapter.

1.1 Background

Indonesia is one of top five coal producers in the world along with China, the United States, India and Australia [1,2]. Hence, coal and mineral production is still one of the largest non-tax revenues of Indonesia [3]. Most Indonesian coal mining company apply open pit mining due to its effectiveness, safety, and lower cost. However, open pit mining causes some environmental problem such as acid mine drainage (AMD), land movement, soil erosion, sedimentation, and toxicity [4,5]. Acid mine drainage is wastewater generated when the sulfide minerals (M), such as: pyrite (FeS_2), Alabandite (MnS), Galena (PbS), Sphalerite (ZnS), etc., are exposed with oxygen and water (Eq. (1.1)). This wastewater typically has low or near neutral pH.

$$2(M)S_2 + 7O_2 + 2H_2O \rightarrow 2(M)^{2+} + 4SO_4^{2-} + 4H^+ \quad (1.1)$$

The sulfide minerals are commonly present in coal bed formation as impurities. When the overburden is excavated, the sulfide minerals in the coal bed are exposed to the atmosphere and rainfall or groundwater (Fig. 1.1). Some metals such as iron, manganese, aluminum, etc., and also other heavy metals with elevated concentration are possibly containing in AMD [6]. The presence of metal types is not always together and depends

on geological condition.

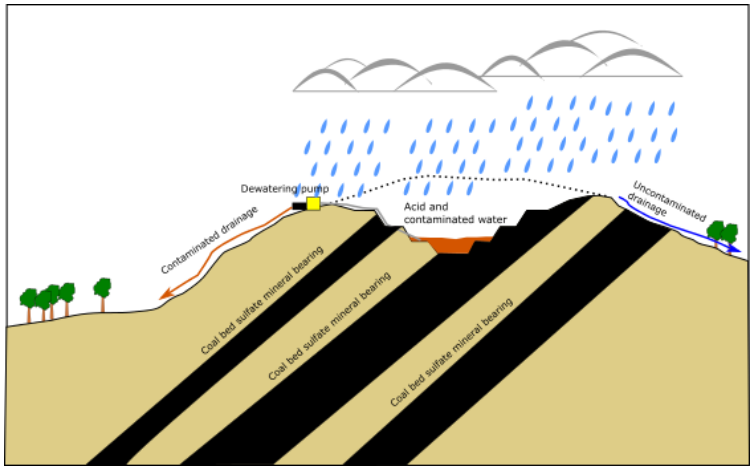

Fig. 1. 1 Sulfide minerals in the coal bed which are exposed to the air and rainfall in open-pit mining.

1.2 Indonesian AMD characterization (a field case study)

One of Indonesian coal mining company, PT. Jorong Barutama Greston which is located in Jorong, Tanah Laut district, Province of South Kalimantan, Indonesia, exhibited containing two metal types in the AMD: Mn and Fe [7]. The data was taken from several voids (mining pit) and showed concentration range 1.7 – 27.2 mg/L for Mn and 0.04 - 3.44 mg/L for Fe with pH 2.54 - 3.41 [7].

Indonesian government set the maximum limit of concentration in mining waste is 4 mg/L for Mn and 7 mg/L for Fe [8,9]. These maximum limits are higher than the quality standard for drinking water since the remediated mining waste usually only used for such as irrigation, agricultural purpose, fish cultivation and not for drinking water.

The Fe concentration contained in AMD at PT. Jorong Barutama Greston coal mining company is still below the maximum limit of standard quality. Meanwhile, the Mn exceeded the quality standard. Manganese itself even though is not as ecotoxic as other metals and one of essential elements for human body, but elevated concentration of manganese can cause serious problem and diseases such as children hyperactive

syndrome, parkinson-like disorder, and neurological symptom due to chronic manganese poisoning [10,11].

1.3 AMD treatment methods

Treatment of AMD mainly is divided into two types “active” method and “passive” method, where both methods possibly involving physical, chemical, and biological process, and either has same main purposes to decrease the metal toxic and raise the pH [6].

Active treatment means the method always involves human assistance to add reagent to neutralize the pH and remove the metal. Active treatment method requires fixed plant to run the operation (Fig. 1.2). One common example of active method types is low-density sludge (LDS) which involve three steps: mixing of reagent and dosing step; reaction step; flocculation and clarification step (Fig. 1.3). [12].

Passive treatment, contrary to active, this method only needs occasionally human assistance. In principle, the AMD is passed through to the passive system installation such as anoxic/oxic limestone, and aerobic/anaerobic. Hence, this method does not need continuous reagent addition [6,12,13]. One common example of passive method type is limestone channel (Fig. 1.4).

Fig. 1. 2 Low density sludge fixed plant [12].

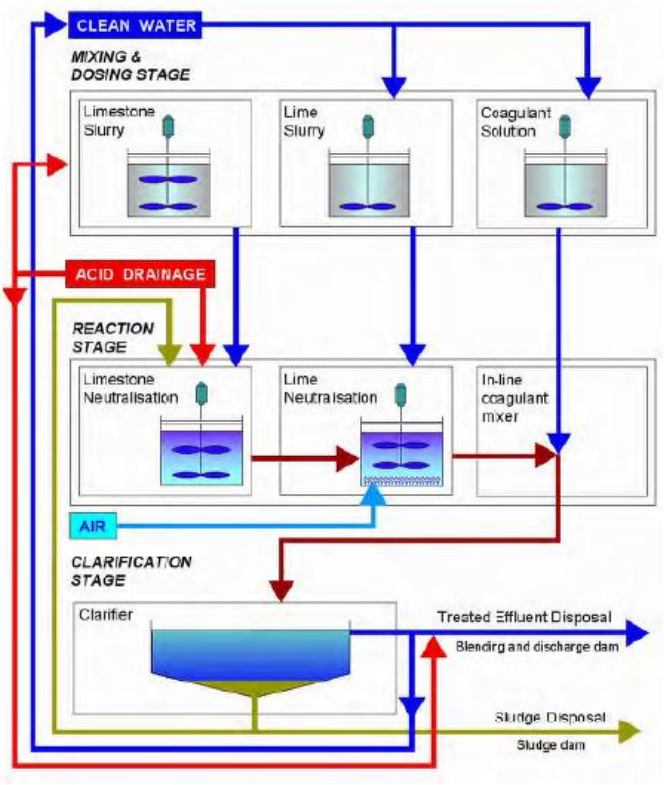

Fig. 1. 3 Flow diagram of LDS in active method of AMD treatment [12].

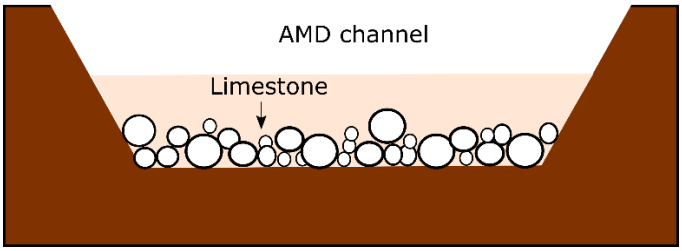

Fig. 1. 4 Cross sectional side view of limestone channel in AMD passive treatment.

Passive treatment method is more economical compared to active treatment method. However, passive method can only handle low volume and flow rate, low concentration of metals, and mild acidity [12]. For instance, in carbonate-based system not all metals can be removed due to maximum pH limitations that can be reached (e.g. Manganese cannot be removed completely) [12]. While in aerobic wetlands system, even though successfully precipitate Fe 60-95%, it can only precipitate Mn less than 10% [12]. Like other passive treatment methods, anaerobic wetlands can only remove limited Mn, unless it is applied in very large areas [13].

1.4 Potential of natural clay bentonite

Bentonite, natural clay material that has been widely used as a low-cost sorbent is selected as an alternative AMD remediation material in this research. General theory of bentonite will be presented in this sub chapter. Before the bentonite explanation, brief explanation about clay will be presented first.

1.4.1 Clay and clay minerals

The term “clay” is differentiated from “clay mineral”. Even though there are many suggested definitions, in general term “clay” refers to natural material which has fine-particle size <4 μm (the Udden-Wenworth scale classification), earthy, and plastic [14,15]. While “clay mineral” is described as phyllosilicate mineral, essential constituent of clay, which contributes the plasticity to clay after moisturized and hardening after drying or firing [16,17]. However, clay material possibly contain non-clay mineral as well [14].

Clay minerals are built from two distinct structural units tetrahedron and octahedron. The tetrahedron is an arrangement where a silicon atom positioned in the center coordinated to four oxygens with the same distance (Fig. 1.5). The tetrahedron is the foundation of silicate structure. The octahedron consists of six closely packed oxygens or hydroxyls ion in which, aluminum, iron, or magnesium positioned in the center with same distance from oxygens or hydroxyls (Fig. 1.6). The stack patterns of these two basic units and the type of center atom, will determine the classification and nomenclature of clay mineral.

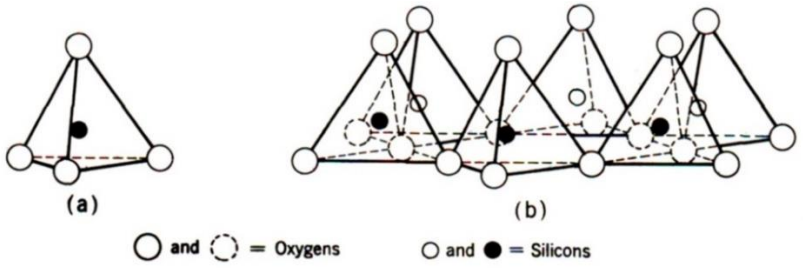

Fig. 1. 5 (a) A single tetrahedron (b) tetrahedrons in sheet [14].

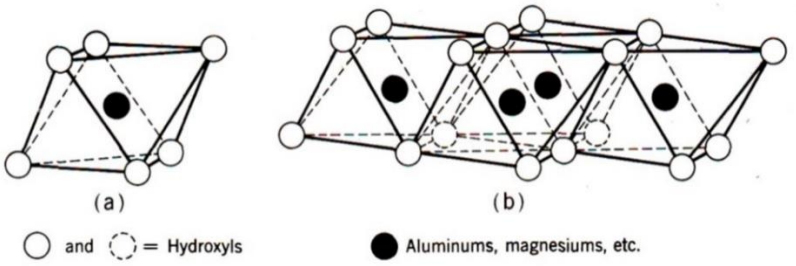

Fig. 1. 6 (a) A single octahedron (b) octahedrons in sheet [14].

Many different classifications were already described. However, Nomenclature and Classification Committee of Association Internationale pour L'Etude des Argiles (A.I.P.E.A) proposed classification scheme for the phyllosilicate to the International Mineralogical Association which seems the closest approach the clay mineralogists. The AIPEA Nomenclature Committee separated the phyllosilicate into hierarchical system of mineral *type*, *group*, *subgroup*, and *species* (Table 1.1).

The type classifications are based on the layer structure of clay minerals 1:1, 2:1, and 2:1:1 (Fig. 1.7). Type 1:1 is the simplest phyllosilicate structure, the layer consists of one tetrahedral sheet and one octahedral sheet. The distinguishing within the subgroup in 1:1 type is the octahedral occupation. Dioctahedral is for kaolinite and trioctahedral is for serpentine [18]. The species are differentiated by such as crystal morphology and water molecule presence [18,19].

Table 1.1 Phyllosilicate classification scheme proposed by Nomenclature Committee of AIPEA [14].

Type	*Group* (*x* = *layer charge*)	*Subgroup*	*Species**
	Pyrophyllite-talc	Pyrophyllites	Pyrophyllite
	$x \sim 0$	Talcs	Talc
	Smectite *or* montmorillonite-saponite	Dioctahedral smectites *or* montmorillonites	Montmorillonite, beidellite, nontronite
	$x \sim 0.5 - 1$	Trioctahedral smectites or saponites	Saponite, hectorite, sauconite
	Vermiculite	Dioctahedral vermiculite	Dioctahedral vermiculite
2:1	$x \sim 1 - 1.5$	Trioctahedral vermiculite	Trioctahedral vermiculite
	Mica†	Dioctahedral micas	Muscovite, paragonite
	$x \sim 2$	Trioctahedral micas	Biotite, phlogopite
	Brittle mica	Dioctahedral brittle micas	Margarite
	$x \sim 4$	Trioctahedral brittle micas	Seybertite, xanthophyllite, brandisite
	Chlorite	Dioctahedral chlorites	
2:1:1	x variable	Trioctahedral chlorites	Pennine, clinochlore, prochlorite
	Kaolinite-serpentine	Kaolinites	Kaolinite, halloysite
1:1	$x \sim 0$	Serpentines	Chrysotile, lizardite, antigorite

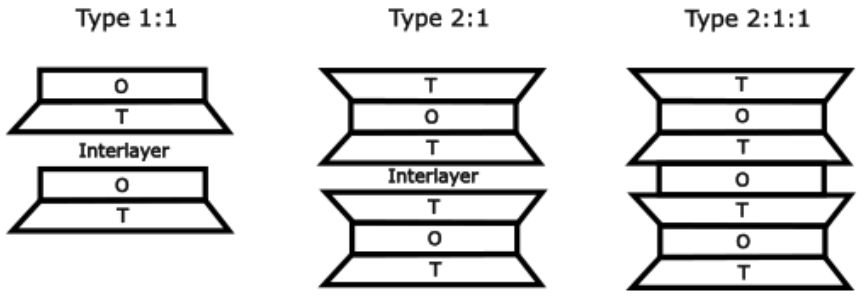

Fig. 1. 7 Clay mineral types 1:1, 2:1, and 2:1:1. T=Octahedral sheet, O=Octahedral sheet.

Type 2:1 means it contains two tetrahedral sheets with one octahedral sheet in between. Within 2:1 type, the group is distinguished by layer charge. The segregation of subgroup is determined by di -or trioctahedral except for pyrophyllite and talc. The difference of ion charge occupied in octahedral sheet distinguishing the species [14,18].

Type 2:1:1 basically has same layer structure with 2:1, but it has octahedral sheet in the interlayer space (brucite or gibbsite). Two layers of hydroxyl cover the center ion

(Al^{3+}, Mg^{2+}, or Fe^{2+}) which bring positive charge. There is no group differentiated by octahedral occupation, interlayer, and interstratification [18].

1.4.2 Bentonite

Bentonite is a term which first applied by Knight in 1898 to a typical, plastic, soapy and highly colloidal clay, found in Cretaceous age bed near Fort Benton [20]. There were several definitions suggested after Knight's definition but the term bentonite is now well defined as any clay which dominantly contains smectite clay mineral whose physical properties governed by this clay mineral [21,22]. In nature, bentonite was formed naturally by devitrification of volcanic ash or hydrothermal alteration [14].

Smectite clay mineral which most contributes to bentonite properties, is including 2:1 type clay mineral (Table 1.1), consisting of an octahedral sheet sandwiched between two tetrahedral silica sheets (Fig. 1.8). All of the tetrahedron tips point toward the center of unit and have the same direction. The tips of tetrahedron are in the same layer with OH^- of octahedron. The layers formed continuously in *a* and *b* directions and stacked in *c* direction. The bonding between sequent layers (interlayer) is Van der walls forces and occupied exchangeable cations. This bond is very weak but with excellent cleavage where water molecule or other polar molecules is able to enter this interlayer and cause expanding lattice in *c* direction. The basal spacing $d_{(001)}$ in *c* direction is variable, not fixed, about 9.6 Å without water or polar molecule in interlayer. In hydrated condition, it expands about 15.4 Å – 18 Å for Ca-montmorillonite, and above about 40 Å for na-montmorillonite [23].

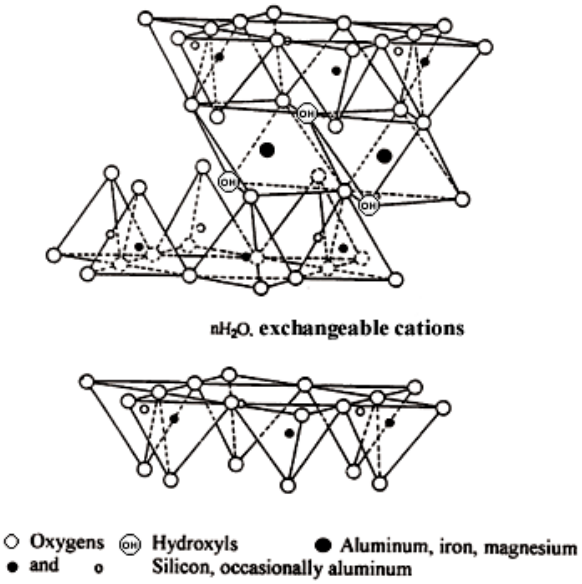

Fig. 1. 8 Schematic of smectite structure [14].

Cation exchange capacity (CEC) is one of basic properties of clay minerals. Cation exchange capacity represented the negative charge per unit mass of clay and expressed as milliequivalent/100 g (meq/100g) [24]. Bentonite has various CEC values range 80-150 meq/100g [25]. Grim (1968) divided the source of cation exchange of smectite mineral into three: a) isomorphic substitution, b) broken edges, and c) the hydrogen of hydroxyl exposed [14] which are described as follows:

a. Isomorphic substitution

Isomorphic substitution refers to permanent charge of mineral that developed during mineral formation from liquid magma or precipitates from a supersaturated solution. This permanent charge, which specific to the phyllosilicates yields negative charge in the mineral bearing [18]. The theoretical formula of 2:1 type without isomorphic substitution is $(OH)_4Si_8Al_4O_{20}$. This theoretical formula is neutral charge and essentially the same as pyrophyllite mineral structure (Fig. 1.9). However, smectite always differs from the theoretical formula due to isomorphic substitution [26,27]. Silicon in tetrahedral sheet is substituted by

aluminum, while aluminum in octahedral sheet can be substituted by magnesium, iron, zinc, nickel, lithium, etc. [14]. The substitution can be one for one or three for two cations. For example, in octahedral sheet substitution of one Mg^{2+} for one Al^{3+} or three Mg^{2+} for two Al^{3+}. The first example causes deficiency of cation and increase a net negative charge and will be balanced by the cation from interlayer [14,18,28]. This deficiency also occurs in the tetrahedral sheet when Si^{4+} is substituted by Al^{3+}. Cation type, charge, amount, which substitute the Al^{+3} in the octahedral sheet, and the substitution occurrence in the tetrahedral sheet determine the subgroup and species of smectite mineral. In smectite minerals which always have negative charge, the substitution can occur: in both tetrahedron and octahedron, only in octahedron, or only tetrahedron. For instance, substitution of $3Mg^{2+}$ for $2Al^{3+}$ with also substitution Al^{3+} for Si^{4+} yields saponite; substitution of Fe^{3+} for Al^{3+} with also substitution Al^{3+} for Si^{4+} yields nontronite; substitution of Mg^{2+} without substitution Al^{3+} for Si^{4+} yields montmorillonite; substitution of Zn^{2+} with also substitution Al^{3+} for Si^{4+} yields sauconite; substitution only Al^{3+} for Si^{4+} (without octahedron) yields beidellite [14,18,28]. Some smectite minerals and its ionic substitution are listed in Table 1.2.

The charge deficiencies of montmorillonite, the most common mineral of the group, due to these isomorphic substitutions has range from 0.5 to 1.2 per unit cell. But generally, the charge deficiency is 0.66 per unit cell which would result from replacement of every sixth aluminum by single magnesium ion. Theoretically, the 0.66 Mg deficiency would be satisfied by 0.66 Na [28]. The formulas mentioned in Table 1.2 should be considered indicative of the general character of the mineral, but not as absolute, because a variety of compositions can exist within the same basic crystal structure.

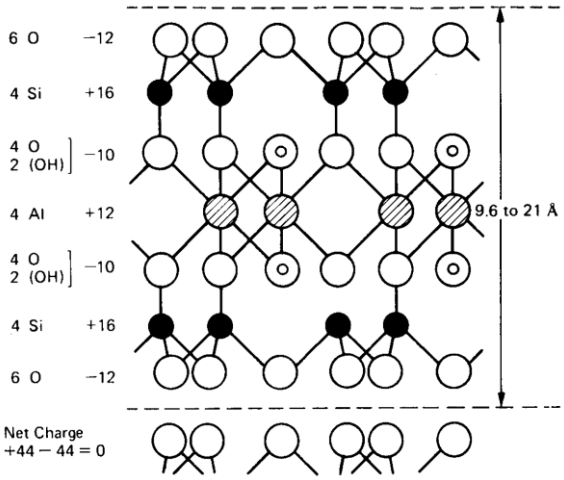

Fig. 1. 9 Pyrophyllite charge distribution (structure type of smectite) [28].

Table 1.2 Several minerals of smectite groups and the ionic substitution [29–31] .

Type	Group	Subgroup	Species	Tetrahedral sheet substitution	Octahedral sheet substitution	Formula /unit cell
2:1	Smectite	Dioctahedral smectite	Montmorillonite	None	1 Mg2+ for every sixth Al^{+3}	$(OH)_4Si_8(Al_{3.34}Mg_{0.66})O_{20}$
			Beidellite	Al for Si	None	$(OH)_4(Si_{6.34}Al_{1.66})Al_{4.34}O_{20}$
			Nontronite	Al for Si	Fe^{+3} for Al	$(OH)_4(Si_{7.34}Al_{0.66})Fe_4^{3+}O_{20}$
		Trioctahedral smectite	Hectorite	None	Li for Mg	$(OH)_4Si_8(Mg_{5.34}Li_{0.66})O_{20}$
			Saponite	Al for Si	Fe^{3+} for Mg	$(OH)_4(Si_{7.34}Al_{0.66})Mg_6O_{20}$
			Sauconite	Al for Si	Zn for Mg	$(OH)_4(Si_{8-y}Al_y)(Zn_{6-x}Mg_x)O_{20}$

b. Broken bonds

Broken bonds occurred around the edges of the silica-alumina units causes the raise of unsatisfied charges, and will be balanced by adsorbed cations (Fig. 1.10) [14]. The exchange capacity due to the number of broken bonds would increase as the particle decreased. The lattice distortions also would tend to increase the

broken bonds, and raise the exchange capacity as the degree of crystallinity decreased. However, in smectites, broken bonds only contribute relatively small portion (±20%) of cation exchange, the rest probably from isomorphic substitution within the lattice [14].

c. The hydrogen of exposed hydroxyls

This cause is typical for kaolinite and halloysite because of the presence of the hydroxyl sheets on one side of the basal cleavage. McConnell (1950) suggested an alternative structure of smectite which had hydroxyls in basal plane cleavage surfaces [32]. Based on this structural concept, cation exchange capacity of smectite exists. However, this concept generally is not accepted [14].

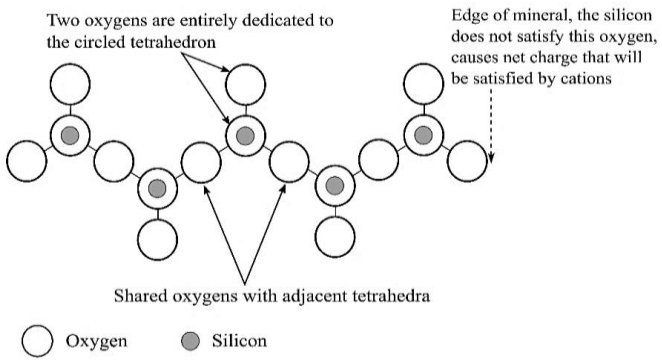

Fig. 1. 10 Schematic of broken bonds from bottom view of tetrahedral layer (adapted from Grim, 1968) [14].

Many methods have been conducted to measure the surface area of clay. The most reliable results have been developed by Brunauer, Emmett, and Teller [33,34], which relies on the adsorption of simple molecules, such as nitrogen, at temperatures of their boiling point in the neighborhood. Clay materials are composed of fine-grained clay and other colloidal phases which has large surface area and significantly affect its properties. Clay minerals have various surface area for smectite is reported between around 5 – 130

m^2/g [35–39]. These surface areas reflect the external and internal surface areas which are a function of their crystal size and a function of mineral type [40]. The external and internal surface area of smectite depicted in Fig. 1.11.

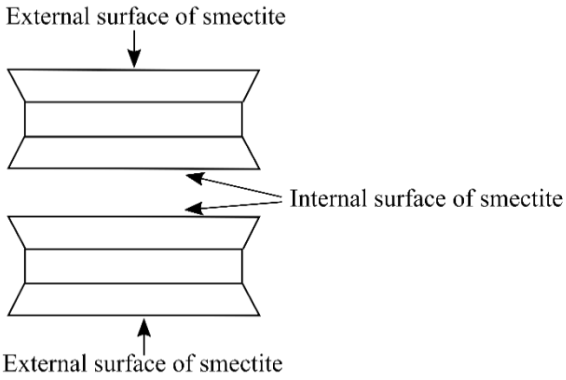

Fig. 1. 11 Schematic illustration of external and internal surface area of smectite (modified from Eslinger and Pevear, 1988) [41].

Most of clay minerals are not only composed of one mineral type. Clay minerals are usually mixed with another clay minerals or composed interstratified layers of different composition [14,42]. The interstratified composition may be regularly or randomly [14,42]. The former means the array along the *c* axis is a regular repetition of different layer of clay mineral and the later means there is no uniform repetition of layers [14,42]. In smectite, the mixed-layer minerals are common as illite-smectite and chlorite-smectite [42,43]. The mixed-layer minerals can be formed by hydrothermal origin (most frequent) or weathering [42,43]. It is reported the mixed-layer in smectite affecting lower CEC compared to the non-mixed layer, around 10-70 meq/100 g for illite-smectite and 20-40 meq/100 g for chlorite-smectite [42]. The illustration of mixed-layer mineral shown in Fig. 1.12.

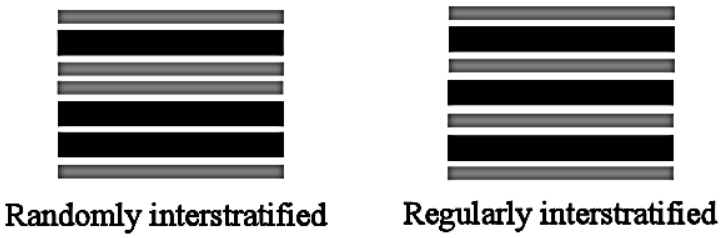

Fig. 1. 12 Types of mixed-layering (modified from Nadeau et al, 1984) [43].

As the smectite has negative surface charge due to isomorphic substitution of cations by less positive cations, the unsatisfied negative charged is compensated by cations located on the surface of clay. When the water presents, the compensating cations tend to diffuse away from the surface layer. On the other hand, higher concentrations of anions tends to diffuse toward the surface layer. This behavior of cations and anions tendency to be repelled or attracted by surface layer, diffuse away from or toward the surface layer is called diffuse double layer. This double layer has constant charge in static environment, and dominantly determined by isomorphic substitution degree and the resulting negative charge in surface layer [44]. This diffuse tendency is depicted in Fig. 1.13.

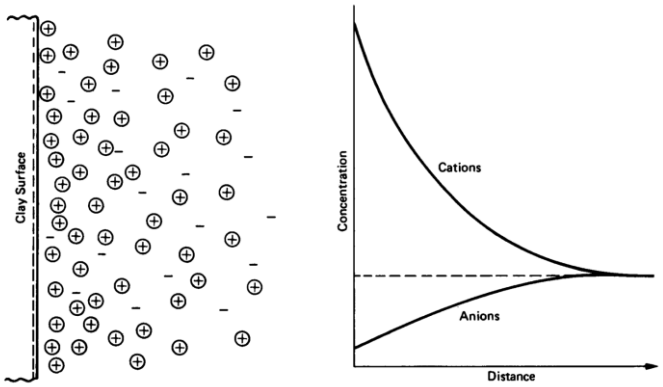

Fig. 1. 13 Diffuse double layer concept, describing distributions of ions adjacent to a surface layer of clay [28].

Some modifications have been developed to improve bentonite sorption performance such as acid activation, pillaring, and milling [45–49]. Milling itself is mechanically modification technique by applying impact on the sample (Fig. 1.14). Milling on bentonite leads to morphological change, partial destruction, rounded edges in particles, particle size reduction, structural peeling and exfoliation, which all could increase the SSA, microporosity, and CEC [38,48,50–52]. Specific surface area (SSA) and cation exchange capacity (CEC) are two components perform important role for sorbent [53,54]. Some studies reported milling-activated bentonite which brought an increase in SSA and CEC had satisfying results for metals removal [47,48,55]. However, prolonged milling will cause a decrease in SSA and CEC. Particle agglomeration is the one responsible for the SSA and microporosity decrease, while amorphization and layer charge decrease are responsible for the CEC decrease [38,56].

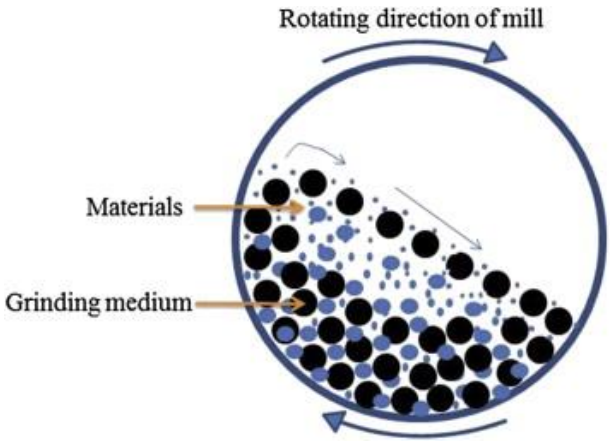

Fig. 1. 14 Schematic diagram of rotary ball miller [57].

1.5 Batch sorption

Sorption is a term used to represent every type of substance capture from the external surface of solids, liquids, or mesomorphs and also from the internal surface of porous solids or liquids which can be divided into physisorption, chemisorption, and ion

exchange [58]. Sorption term often simply used for the removal of soluble compound from solution phase process, especially when only the substance mass disappearance is determined without mechanism implied because the specific retention process is not known [18]. On the other hand, the term “adsorption” means liquid or gaseous components uptake of mixtures from the external and/or internal surface of porous solids [59]. In chemical engineering, the term "adsorption" means separation process of specific components from liquid phase transferred to the solid surface of the adsorbent [60].

Some literature mentioned ion exchange is similar to adsorption, with the reason there is mass transfer from liquid to solid phase in both processes [18,59]. Other authors differentiate between adsorption and ion exchange since in ion exchange process, the ions are adsorbed to the surface. While in adsorption the electrically neutral species are adsorbed [61,62]. In soil chemistry, that adsorption is similar ion exchange is used [18]. However, it is generally accepted that adsorption and ion exchange are grouped together as sorption for unified treatment in practical application [59].

Sorption isotherms are commonly used to obtain parameter of compound-specific adsorption that quantitatively describes adsorption in a specific environment [18]. Hence, sorption isotherms should be described in mathematical description. These sorption isotherms are obtained using laboratory batch test, by mixing the water containing the constituent at certain concentration with the solid and allowing the mixture reach equilibrium [63]. By conducting the same tests in various concentrations of constituent with the same temperature, a relation between sorbed mass (q) and equilibrium concentration (C_e) is obtained. Where q can be obtained:

$$qe = \frac{C_0 - C_e}{m} V \tag{1.2}$$

where *qe* is sorbed substance on sample (mg/g), *Co* is initial concentration (mg/L), *Ce* is Final Concentration (mg/L), *V* is solution volume (ml), *m* is sample mass (g)

The sorption isotherms are described in some mathematical models. The most common used is Langmuir. The Langmuir is developed from theoretical based. In soil chemistry, the Langmuir is developed for the adsorption of a solute from an aqueous environment and assumes solute adsorption is an exchange process that occurs at specific sites on a homogeneous surface. The adsorbed solute formed monolayer on the surface and reached the maximum adsorption as the monolayer becomes saturated by the adsorbate [18]. The Langmuir equation is:

$$qe = \frac{Q_m k_L C_e}{1 + kC_e} \tag{1.3}$$

where Q_m is adsorption maxima, and k_L is Langmuir constant.

Another model can be used Brunauer, Emmet, and Teller (BET). The BET model is an extension of the Langmuir theory, which is a theory of monolayer molecular adsorption, to multilayer adsorption. This model is originally developed for gas adsorption, and recently is applied for the liquid phase adsorption. The equation of BET in liquid phase can be expressed as:

$$qe = \frac{(Qmax.k_B.C_o.C_e)}{(C_o - C_e)}[C + (k_B - 1)C_e] \tag{1.4}$$

1.6 Column sorption

It is common in industrial, wastewater treatment to pass the waste through a column packed with a sorbent inside to be treated. This bed sorption column is more complicated than the simple stirred tank batch mechanism which reaches equilibrium. The whole dynamics in this system determines the efficiency of the operation rather than just equilibrium parameters [64]. The transport process in the bed is illustrated in Fig. 1.15. The top of the curve at t_1 describes the contact of the bed with the solution at the highest concentration and gradually decrease downward until zero. Hence, it has clean

water in the effluent. The length in the bed where the concentration gradually changes is called the mass transfer zone (*MTZ*). As the time continues and solution passes through, this first zone will be saturated, and the contact with the solution will move to fresher sorbent in the next layer or zone at t_2. The movement which generates clean water in the effluent will continue until t_4. The last zone at t_5 the sorbent is no longer capable of generating clean water as before. The concentration in effluent starts to increase. The condition at this point is called as breakthrough time. If the flowing solution still continue the concentration in the effluent will gradually increase and reach the condition where the concentration in the effluent has same value within the influent. This concept can be described as breakthrough curve in Fig. 1.16. When the breakthrough occurs, consequently there is amount of sorbent in the bed cannot be used. In column sorption operation evaluation this unused amount is stated as length of unused bed (*LUB*).

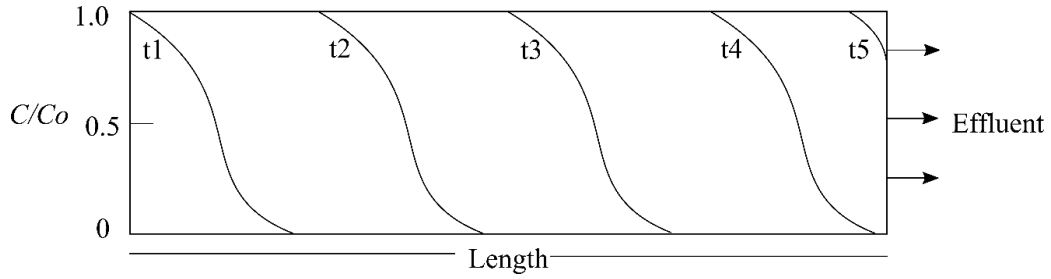

Fig. 1. 15 Concentration of sorbate profile at various position and times in sorbent bed (modified from Geankoplis, 1993) [64].

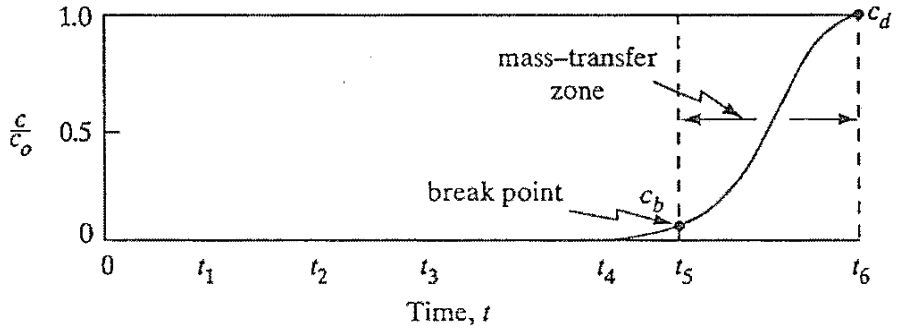

Fig. 1. 16 Breakthrough curves [64].

Since the experimental of column sorption test gives discrete data, the mathematical models to predict the breakthrough curve and the concentration at any time during operation are needed. Some common developed models are Thomas, Adams-Bohart, and Yoon-Nelson.

Thomas model is widely used to determine rate constant and maximum adsorption capacity in column. Thomas (1944) derived this model from Langmuir kinetics at equilibrium and neglects axial and radial dispersion [65]. The local rate adsorption is assumed:

$$\frac{\partial q}{\partial t} = k[C(q_{max} - q) - b(C_o - C)] \tag{1.5}$$

It considers the rate as a chemical reaction whose rate is governed by mass action and with the concentrations uniform along the adsorbent. Hence, when the rate approaches zero at equilibrium, the equilibrium conditions become those of the Langmuir isotherms since the expression of rate is in principle the same as that used in the Langmuir isotherms [66]. The Thomas solution is written as:

$$\frac{C_t}{C_0} = \frac{1}{1 + exp\left[\left(\frac{k_{Th} q_0 m}{v}\right) - k_{Th} C_0 t\right]} \tag{1.6}$$

k_{Th} = Thomas rate constant (L/min.mg), q_0 = equilibrium uptake of sorbate (mg/g), m = mass of sorbent (g), C_0 = influent concentration (mg/L), C_t = effluent concentration at time (t) (min), v = flow rate (mL/min).

Adams-Bohart model assumes that both the residual capacity and the concentration of the sorbing species are proportional to the adsorption rate [67]. Adams and Bohart used the quasichemical rate law:

$$\frac{\partial q}{\partial t} = kC(q_s - q) \tag{1.7}$$

q_s is the constant value of q referring to horizontal line of the isotherm in Fig. 1.17. Note this rate law suggests that at equilibrium rate =0, q=qs, for any value of C. The Adams-Bohart equation is expressed as follows:

$$\frac{C_t}{C_0} = \frac{\exp(k_{AB} C_t t)}{exp\left[k_{AB} N_0 \left(\frac{H}{U_0}\right)\right] - 1 + exp(k_{AB} C_0 t)} \tag{1.8}$$

where, k_{AB} = kinetic constant (L/mg.min), N_0 = saturation concentration (mg/L), U_0 = linier velocity (cm/min), H = depth of bed (cm). The Adams-Bohart model is suited to describe until the initial part of breakthrough.

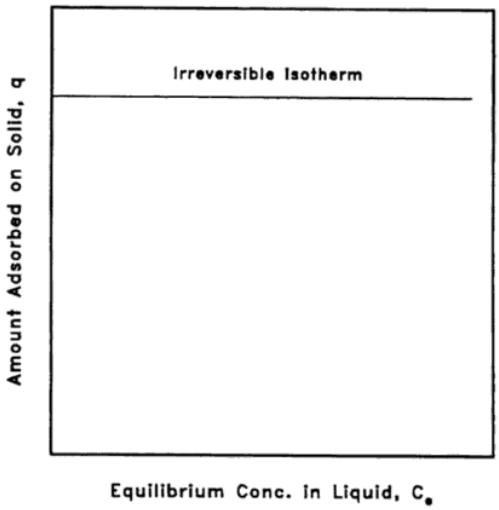

Fig. 1. 17 Isotherm shape of irreversible isotherm [68].

Yoon-Nelson model mathematically analogous from Thomas model. Yoon-Nelson assumes the rate of adsorption decrease for each molecule in the probability is proportional to the probability of the adsorbate adsorption and the adsorbate breakthrough on the adsorbent [69]. This model is simple and does not require any detailed data relates to adsorbate and adsorbent characteristics and the phisycal properties of bed sorbent. The Yoon-Nelson solution is:

$$\frac{C_t}{C_0} = \frac{1}{1 + exp[k_{YN}(t_{50} - t)]} \tag{1.9}$$

where k_{YN} = the Yoon–Nelson rate constant (L/min), τ = the time in required for 50% sorbate breakthrough (min).

1.7 Problem statement

Even though milled bentonite has improved the removal of metal, however the optimization of milling investigation and its character identification to achieve the maximum sorption performance for metal removal, as long as author's knowledge never investigated before. Previous studies only performed one milling condition and directly applied to metal sorbent.

As the milling modified bentonite has big potential for metal removal, however application of milling modified bentonite for bed sorbent as passive treatment of AMD never conducted before.

PT. Jorong Barutama Greston coal mining company contained two metal types in the AMD: Mn and Fe which the Mn has exceed concentration. In the low-cost passive treatment method that utilizes the carbonate-based system, Mn is still a problem since it requires higher pH to be precipitated.

1.8 Objectives

The main aim of this study is to apply milled bentonite as a bed sorbent in AMD passive treatment. The material used is natural bentonite from central Java, Indonesia and named as **Indonesian natural bentonite (INB)** (The overview of INB will be presented in chapter 2). The specific objectives of this research are:

1. To optimize the milling time on INB for manganese removal from AMD and increase the pH.
2. To identify the character of optimized ball-milled INB.

3. To study the significance improvement of optimized ball-milled INB on column sorption test as AMD passive treatment approach.

To achieve the main and specific objectives above the work order is described as below:

1. Characteristic change investigation of INB during continuous milling. This investigation observes every characteristic change of INB with the increase of milling time at certain interval time. This part is presented in chapter 3.
2. Batch sorption test to select the highest adsorption capacity. The selected samples in this batch test are based on the significant character change in point 1. The characteristic of INB when It reaches the highest sorption capacity can be identified by referring to the result at point 1. This part is presented in chapter 4.
3. Column sorption test using selected milled INB (the highest sorption capacity at point 2) and also the comparison with the unmilled. This part is presented in chapter 5.

The flowchart of this work order is depicted in Fig. 1.18.

1.9 Scope and limitations

1. Characteristics of INB and its change during continues milling modification observed are limited to mineral presence, morphology, crystal structure change of montmorillonite, specific surface area, microporosity, cation exchange capacity, and particle size.
2. The highest adsorption capacity investigation only for manganese which simulated from the AMD of PT. Jorong Barutama Greston coal mining company. The metal is limited on Mn since the Fe is still below the maximum limit of quality standard and besides Fe tends to be easily precipitated.

3. Column sorption test focuses on the improvement of maximum Mn sorbed on bed (q), breakthrough time (b_t), and length of unused bed (LUB) before and after ball-milling modification in constant flow rate. This column sorption does not quantify the geotechnical properties such as hydraulic conductivity change, swelling behavior, etc., during experiment since the sample only in small mass in fixed bed column and only use small-scale vacuum chamber equipment.

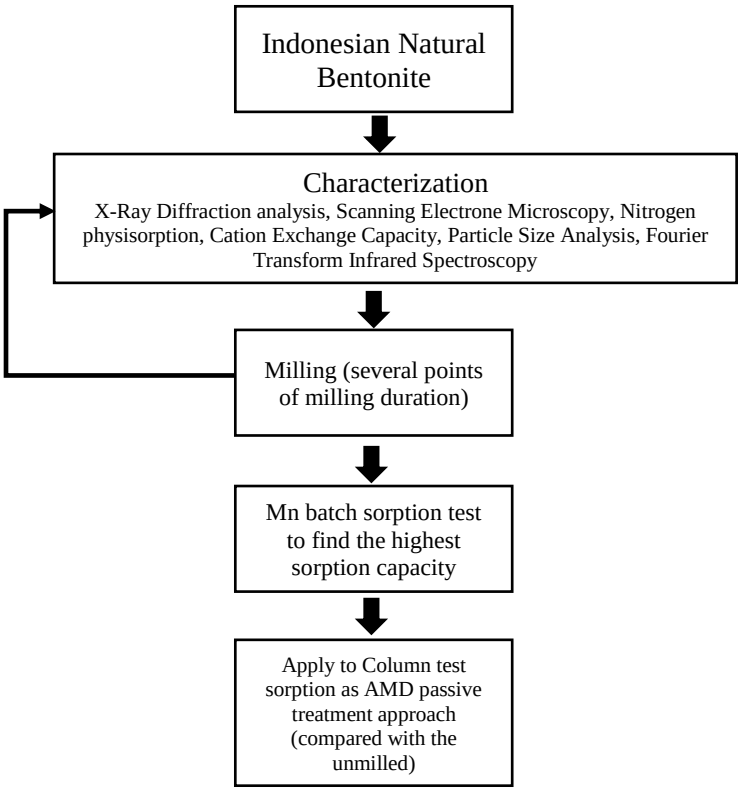

Fig. 1. 18 Research flowline.

This dissertation is divided into 6 chapters, and brief description of each chapter described as follows:

Chapter 1: This chapter provides brief explanation about: acid mine drainage (AMD) and its environmental concern; bentonite review, its optimizing ball-milling modification challenge, and the potential as AMD remediation material; batch and column sorption test review. Objectives and research limitation are presented in the last

section of this chapter.

Chapter 2: General initial information about Indonesian natural bentonite (INB) are presented in this chapter. Sampling location, resource potential, geological condition, brief explanation about characteristics and properties such as mineral presence and geotechnical information from author's side and previous research are given in order to give basic understanding about the natural clay bentonite condition used in this research.

Chapter 3: Morphological change, microstructural modification and deformation, change of specific surface area, microporosity, cation exchange capacity during, and particle size distribution during continues ball-milling are presented and explained in detail in this chapter.

Chapter 4: The effect of ball-milling on Indonesian natural bentonite (INB) for Mn sorption is elucidated through batch sorption test effect of contact time. The highest sorption capacity is selected for next experiment: effect of different sorbate concentration and effect of different pH. Mathematical model the Langmuir and Brunauer, Emmet, and Teller (BET) model are also described.

Chapter 5: Application of effective milled Indonesian natural bentonite (INB) on fixed-bed column sorption is presented in this chapter. Mass transfer zone (*MTZ*), length of unused bed (*LUB*), and mathematical model of Thomas, Adams-Bohart, and Yoon-Nelson are explained. The explanation presents comparation between unmilled INB and after milling modification.

Chapter 6: This chapter describes the general conclusions derived from this study.

References

[1] World Energy Council, World Energy Resources Coal, 2016.

[2] International Energy Agency, Coal Information: Overview, 2017.

[3] The World Bank, Penerimaan Negara Bukan Pajak dari Pertambangan di Indonesia, 2014.

[4] S. Maryati, H. Shimada, A. Hamanaka, T. Sasaoka, K. Matsui, Determine Appropriate Post Mining Land Use in Indonesia Coal Mining Using Land Suitability Evaluation, J. Nov. Carbon Resour. Sci. 5 (2012) 33–38.

[5] A. Akcil, S. Koldas, Acid Mine Drainage (AMD): causes, treatment and case studies, J. Clean. Prod. 14 (2006) 1139–1145. doi:10.1016/j.jclepro.2004.09.006.

[6] D.B. Johnson, K.B. Hallberg, Acid mine drainage remediation options: A review, Sci. Total Environ. 338 (2005) 3–14. doi:10.1016/j.scitotenv.2004.09.002.

[7] Herniwanti, J.B. Priatmadi, B. Yanuwiadi, Soemarno, Characteristics of acid mine water, Int. J. ChemTech Res. 6 (2014) 967–972.

[8] Indonesian Government, Government regulation number 82 year 2001 about water quality management and waste water control, Indonesia, 2001. doi:10.1017/CBO9781107415324.004.

[9] Indonesian Ministry of Life Environment, Standar quality for coal mining waste water, Indonesia, 2003. doi:10.1017/CBO9781107415324.004.

[10] M. Bouchard, F. Laforest, L. Vandelac, D. Bellinger, D. Mergler, Hair manganese and hyperactive behaviors: Pilot study of school-age children exposed through tap water, Environ. Health Perspect. 115 (2007) 122–127. doi:10.1289/ehp.9504.

[11] X.G. Kondakis, N. Makris, M. Leotsinidis, M. Prinou, T. Papapetropoulos, Possible health effects of high manganese concentration in drinking water., Arch.

Environ. Health. 44 (1989) 175–178. doi:10.1080/00039896.1989.9935883.

[12] J. Taylor, S. Pape, N. Murphy, A Summary of Passive and Active Treatment Technologies for Acid and Metalliferous Drainage (AMD), in: Proc. 5th Aust. Work. Acid Drain., 2005: pp. 1–49.

[13] C. Zipper, J. Skousen, C. Jage, Passive treatment of acid-mine drainage, Virginia Coop. Ext. 23 (2011) 1338–1345. doi:10.2134/jeq1994.00472425002300060030x.

[14] R.E. Grim, Clay Mineralogy, McGraw Hill Book Company, 1968.

[15] G. Nichols, Sedimentology and Stratigraphy, Wiley-Blackwell, 2009.

[16] T. Al-Ani, O. Sarapaa, Clay and clay mineralogy, Geological Survey of Finland, 2008.

[17] D.M. Moore, Comment on: Definition of Clay and Clay Mineral: Joint Report of the Aipea Nomenclature and Cms Nomenclature Committees, Clays Clay Miner. 44 (1996) 710–712. doi:10.1346/CCMN.1996.0440515.

[18] M.E. Essington, Soil and Water Chemistry: An integrative approach, CRC Press, 2004. doi:10.1017/CBO9781107415324.004.

[19] B. Bauluz, Halloysite and kaolinite: two clay minerals with geological and technological importance, Rev. Real Acad. Ciencias. Zaragoza. 70 (2015) 7–38.

[20] W.C. Knight, Bentonite, Eng. Min. J. 66 (1898) 491.

[21] P.C. Wright, The Meandu creek bentonite-a reply, J. Geol. Soc. Aust. 15 (1968) 347–350.

[22] R.E. Grim, N. Güven, Bentonites: Geology, Mineralogy, Properties and Uses (Developments in Sedimentology), Elsevier Science, 1978.

[23] K. Norrish, The swelling of montmorillonite, Trans. Faraday Soc. 18 (1954) 120–134.

[24] R.E. White, Principles and Practice of Soil Science, Blackwell Publishing, 1979.

[25] R. Pusch, Bentonite Clay: Environmental Properties and Applications, CRC Press, 2015.

[26] C.E. Marshall, Layer Lattices and the Base-Exchange Clays, Zeitschrift Fur Krist. - Cystalline Mater. 91 (1935) 433–449. doi:https://doi.org/10.1524/zkri.1935.91.1433.

[27] S.B. Hendricks, Lattice Structure of Clay Minerals and Some Properties of Clays, J. Geol. 50 (1942) 276–290.

[28] J.K. Mitchell, K. Soga, Fundamentals of Soil Behavior, John Wiley and Sons, Inc, 2005.

[29] C.S. Ross, S.B. Hendricks, Minerals of the montmorillonite group their origin and relation to soils and clays., Geol. Surv. Prof. Pap. 205-B,. (1943) 23–79.

[30] C.E. Marshall, The physical chemistry and mineralogy of soils, Wiley, New York, 1964.

[31] C.M. Marshall, R. Roy, Classification and a Scheme for the Identification of Layer Silicates, Geol. Soc. Am. Bull. 72 (1961) 1455–1492.

[32] D. Mcconnell, The crystal chemistry of montmorillonite, Am. Mineral. 35 (1950) 166–172.

[33] S. Brunauer, P.H. Emmet, The Use of Low Temperature van der Waals Adsorption Isotherms in Determining the Surface Areas of Various Adsorbents, J. Am. Chem. Soc. 59 (1937) 2682–2689. doi:10.1021/ja01291a060.

[34] S. Brunauer, P.H. Emmet, E. Teller, Adsorption of Gases in Multimolecular Layers, J. Am. Chem. Soc. 20 (1938) 309–319. doi:10.1021/ja01269a023.

[35] R. Greene-Kelly, The specific surface areas of montmorillonites, Clay Miner. Bull. 5 (1963) 392–400.

[36] S. Kaufhold, R. Dohrmann, M. Klinkenberg, S. Siegesmund, K. Ufer, N2-BET specific surface area of bentonites, J. Colloid Interface Sci. 349 (2010) 275–282. doi:10.1016/j.jcis.2010.05.018.

[37] N. Vdovic, I. Jurina, S.D. Škapin, I. Sondi, The surface properties of clay minerals modified by intensive dry milling - revisited, Appl. Clay Sci. 48 (2010) 575–580. doi:10.1016/j.clay.2010.03.006.

[38] G.E. Christidis, F. Dellisanti, G. Valdre, P. Makri, Structural modifications of smectites mechanically deformed under controlled conditions, Clay Miner. 40 (2005) 511–522. doi:10.1180/0009855054040188.

[39] J. Thomas, JR., B.F. Bohor, Surface area of montmorillonite from the dynamic sorption of nitrogen and carbon dioxide, Clays Clay Miner. 16 (1968) 83–91.

[40] G.M. Reeves, I. Sims, J.C. Cripps, eds., Clay Materials Used in Construction, Geological Society of London, 2006.

[41] E. Eslinger, D.R. Pevear, Clay minerals for petroleum geologists and engineers, 1988.

[42] C.E. Weaver, L.D. Pollard, Mixed-Layer Clay Minerals, in: Dev. Sedimentol., Elsevier Scientific Publishing Company, 1973: pp. 107–118. doi:https://doi.org/10.1016/S0070-4571(09)70011-1.

[43] P.H. Nadeau, M.J. Wilson, W.J. McHardy, J.M. Tait, Interparticle diffraction : A new concept for interstratified clays, Clay Miner. 19 (1984) 757–769.

[44] R.H. Bennett, R.H. Bennett, W.R. Bryant, M.H. Hulbert, A.H. Bouma, Microstructure of Fine-Grained Sediments: From Mud to Shale, Springer Science & Business Media, 1991.

[45] S. Budsaereechai, K. Kamwialisak, Y. Ngernyen, Adsorption of lead , cadmium and copper on natural and acid activated bentonite clay, KKU Res. J. 17 (2012)

800–810.

[46] M. El Miz, S. Salhi, I. Chraibi, A. El Bachiri, M. Fauconnier, A. Tahani, Characterization and Adsorption Study of Thymol on Pillared Bentonite, Open J. Phys. Chem. 4 (2014) 98–116.

[47] M. Vhahangwele, G.W. Mugera, The potential of ball-milled South African bentonite clay for attenuation of heavy metals from acidic wastewaters: Simultaneous sorption of Co2+, Cu2+, Ni2+, Pb2+, and Zn2+ions, J. Environ. Chem. Eng. 3 (2015) 2416–2425. doi:10.1016/j.jece.2015.08.016.

[48] A. Djukić, U. Jovanović, T. Tuvić, V. Andrić, J. Grbović Novaković, N. Ivanović, L. Matović, The potential of ball-milled Serbian natural clay for removal of heavy metal contaminants from wastewaters: Simultaneous sorption of Ni, Cr, Cd and Pb ions, Ceram. Int. 39 (2013) 7173–7178. doi:10.1016/j.ceramint.2013.02.061.

[49] K.G. Bhattacharyya, S. Sen, Removal of Cu (II) by natural and acid-activated clays : An insight of adsorption isotherm , kinetic and thermodynamics, Desalination. 272 (2011) 66–75. doi:10.1016/j.desal.2011.01.001.

[50] A.R. Ramadan, A.M.K. Esawi, A.A. Gawad, Effect of ball milling on the structure of Na+-montmorillonite and organo-montmorillonite (Cloisite 30B), Appl. Clay Sci. 47 (2010) 196–202. doi:10.1016/j.clay.2009.10.002.

[51] Y.C. Lee, C.L. Kuo, S.B. Wen, C.P. Lin, Changes of organo-montmorillonite by ball-milling in water and kerosene, Appl. Clay Sci. 36 (2007) 265–270. doi:10.1016/j.clay.2006.09.013.

[52] G.E. Christidis, P. Makri, V. Perdikatsis, Influence of grinding on the structure and colour properties of talc, bentonite and calcite white fillers, Clay Miner. 39 (2004) 163–175. doi:10.1180/0009855043920128.

[53] K.G. Bhattacharyya, S. Sen Gupta, Kaolinite, montmorillonite, and their modified derivatives as adsorbents for removal of Cu(II) from aqueous solution, Sep. Purif. Technol. 50 (2006) 388–397. doi:10.1016/j.seppur.2005.12.014.

[54] K.G. Akpomie, F.A. Dawodu, Acid-modified montmorillonite for sorption of sorption heavy metals from automobile effluent, Beni-Suef Univ. J. Basic Appl. Sci. 5 (2016) 1–12. doi:10.1016/j.bjbas.2016.01.003.

[55] V. Masindi, M.W. Gitari, H. Tutu, M. DeBeer, Efficiency of ball milled South African bentonite clay for remediation of acid mine drainage, J. Water Process Eng. 8 (2015) 227–240. doi:10.1016/j.jwpe.2015.11.001.

[56] F. Perrin-Sarazin, M. Sepehr, S. Bouaricha, J. Denault, Potential of Ball Milling to Improve Clay Dispersion in Nanocomposites Florence, Polym. Eng. Sci. 49 (2009) 651. doi:10.1002/pen.

[57] P. Khadka, J. Ro, H. Kim, I. Kim, J.T. Kim, H. Kim, J.M. Cho, G. Yun, J. Lee, Pharmaceutical particle technologies: An approach to improve drug solubility, dissolution and bioavailability, Asian J. Pharm. Sci. 9 (2014) 304–316. doi:10.1016/j.ajps.2014.05.005.

[58] T.N. Skoulikides, Physical Chemistry I 1.2, Symetria Editions, Athens, Greece, 1989.

[59] V.J. Inglezakis, S.G. Poulopoulos, Adsorption, Ion Exchange and Catalysis, Adsorpt. Ion Exch. Catal. (2006). doi:10.1016/B978-0-444-52783-7.X5000-9.

[60] W.L. McCabe, J.C. Smith, P. Harriott, Unit operations of chemical engineering, (1993).

[61] R.D. Noble, P.A. Terry, Principles of Chemical Separations with Environmental Applications, Cambridge University Press, 2004. doi:10.1016/S0009-2509(96)90039-1.

[62] R.H. Perry, D.W. Green, Perry's Chemical Engineer's Handbook, (1999).

[63] L.N. Reddi, H.I. Inyang, Geoenvironmental Engineering Principles and Applications, Marcel Dekker, Inc, 2000.

[64] C.J. Geankoplis, Transport Processes and Unit Operations, Prentice-Hall International, Inc., 1993.

[65] H.C. Thomas, Heterogeneous Ion Exchange in a Flowing System, J. Am. Chem. Soc. 66 (1944) 1664–1666. doi:10.1021/ja01238a017.

[66] J. Watson, Separation Methods for Waste and Environmental Applications, Marcel Dekker, Inc, 1999.

[67] G.S. Bohart, E.Q. Adams, Some aspects of the behaviour of charcoal with respect to chlorine, J. Am. Chem. Soc. (1920). doi:10.1021/ja01448a018.

[68] D.O. Cooney, Adsorption design for wastewater treatment, CRC Press, 1999.

[69] Y.H. Yoon, J.H. Nelson, Application of gas adsorption kinetics, I. A theoretical model for respirator cartridge service life, Am. Ind. Hyg. Assoc. J. 45 (1984) 409–516.

CHAPTER 2
Material used Indonesian natural bentonite overview

General initial information about Indonesian natural bentonite (INB) is presented in this chapter. Sampling location, resource potential, geological condition, brief explanation about characteristics and properties such as mineral presence and geotechnical information from author's side and previous research are given in order to give basic understanding about the natural clay bentonite condition used in this research.

2.1 Location and potential of Indonesian natural bentonite

The material used in this research, Indonesian natural bentonite (INB), is located in Garangan area, Wonosegoro subdistrict, Boyolali district, Central Java, Indonesia (Fig. 2.1). According to Indonesian Ministry of Energy and Mineral Resource (2009), Wonosegoro subdistrict has hypothetical resource of natural bentonite 58 million ton [1]. The 'hypothetical mineral resource' term refers to the early step according to "Criteria and Classification of Mineral Resources and Reserves" defined by national standardization committee of Indonesia [2]. It means the quality and quantity of mineral are based on field reconnaissance or preliminary geological survey and still in the beginning level of geological confidence.

2.2 Field sampling and geological information

The INB was sampled in claystone rock unit in geological outcrop (Fig. 2.2). This claystone rock unit belongs to claystone of Kerek formation which has middle Miocene age (15-10 million years ago) [3]. This representative sampling was conducted based on the similarity of the physical geological description. Hence, one-point sampling in this folded layered sedimentary rock outcrop (Fig 2.3) was considered representing the whole

outcrop in Garangan area. This sampling method is acceptable if the level of geological confidences still at reconnaissance step as mention in the section before. For more detail, certainly sampling using geostatistical approach is needed to raise the geological confidence level and to obtain more detail quality and quantity distribution in this area.

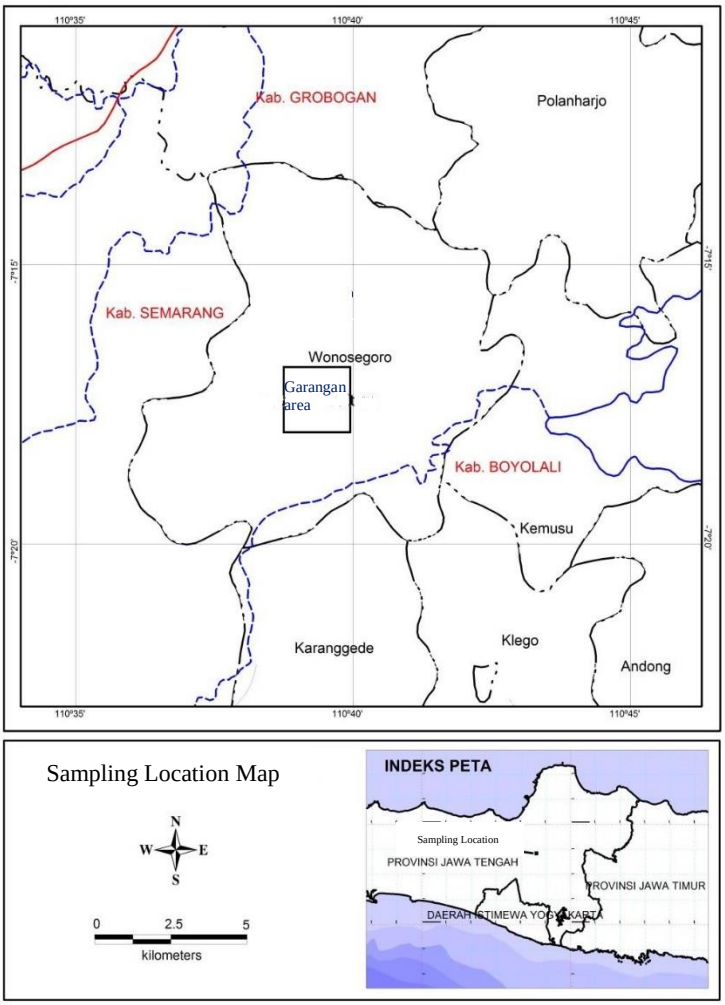

Fig. 2. 1 Sampling location of INB at Garangan area which is part of Wonosegoro sub-district.

Fig. 2. 2 Geological outcrops of Indonesian natural bentonite (INB).

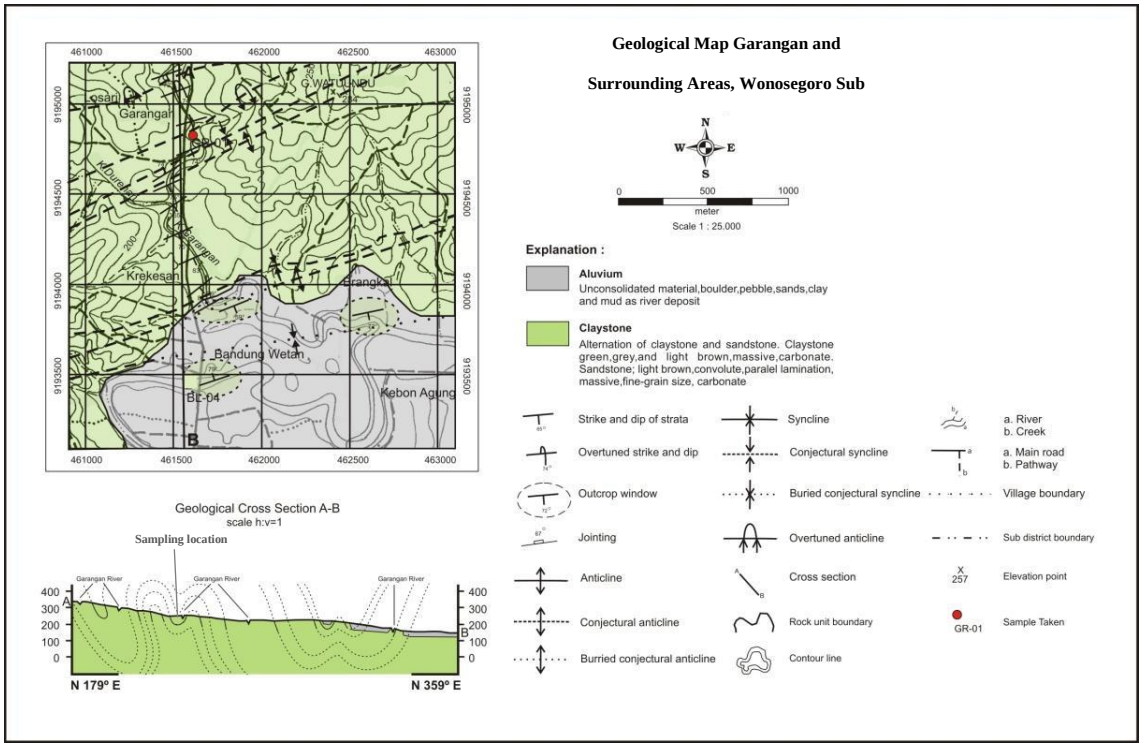

Fig. 2. 3 Geological map of Garangan and surrounding area INB sample taken [4].

2.3 The mineral presence and cation exchange capacity (CEC)

X-ray diffraction (XRD) observation revealed INB has relatively higher intensity of montmorillonite, calcite, and quartz (presented in detail in chapter 3). The cation exchange capacity showed 17.5 meq/100 g (also presented in chapter 3). Another

research, Yulianti (2011) reported based on petrographic observation, the bentonite located ±1 km to the south of INB location, contained a number of volcanic glass that altered to secondary minerals (30-40%), calcite (10-25%), orthoclase (1-10%), quartz (5-20%), plagioclase (0-15%), opaque minerals (5-15%), and lithic (0-5%), while based on XRD measurement contained montmorillonite, kaolinite, and illite. The CEC was reported 20 meq/100 g [5]. The low CEC of bentonite can be explained due to geological process during its formation, a mixed interlayer between the array of montmorillonite [6].

Even though the origin of bentonite in Wonosegoro was predicted as devitrification process [5] which logically has relatively homogenous mineral content, however, the condition after its formation possibly altered due to external process such as weathering. Hence, Yulianti (2011) described some alteration mineral from the mineral identification.

2.4 Geotechnical information

Even though the column sorption test in this research only in small scale and limited to the improvisation of modified bentonite as mentioned in chapter 1, the geotechnical information from the previous study would be useful as initial information of the soil behavior if it is applied in field scale. Several geotechnical information of the initial condition of INB presented in this subchapter are index properties, hydraulic conductivity, and swelling behavior effect.

2.4.1 Index properties

Index properties purpose facilitating identification and classification of soil. The index properties presented are intrinsic properties or atterberg limit and intact properties of INB given in Table 2.1 and Table 2.2.

Table 2.1 Intrinsic properties of INB obtained from slurry condition.

Soil properties	Value
Liquid limit (LL)	57.81%
Plastic limit (PL)	28.32%
Shrinkage limit (SL)	19.30%
Plasticity limit (PL)	29.49%
Specific gravity (SG)	2.69

Table 2.2 Representative intact properties of INB.

Soil properties	Value
Water content (W_c)	22.30 %
Porosity (n)	0.56
Void ratio (e)	1.28
Degree of saturation (S_R)	47

2.4.2 Hydraulic conductivity

The hydraulic conductivity (*K*) measurement was conducted using large-scale column mold (Fig. 2.4), which is close to site condition in various initial water condition. This test was done by seepage from bottom drainage and also conducted during consolidation process with pressure load applied 10, 20, 40, 80, 160, and 245 kPa. The dry condition sample preparation exhibited higher *K* compared to the wet condition (Fig. 2.5). The hydraulic conductivity decreases as the pressure increase [7].

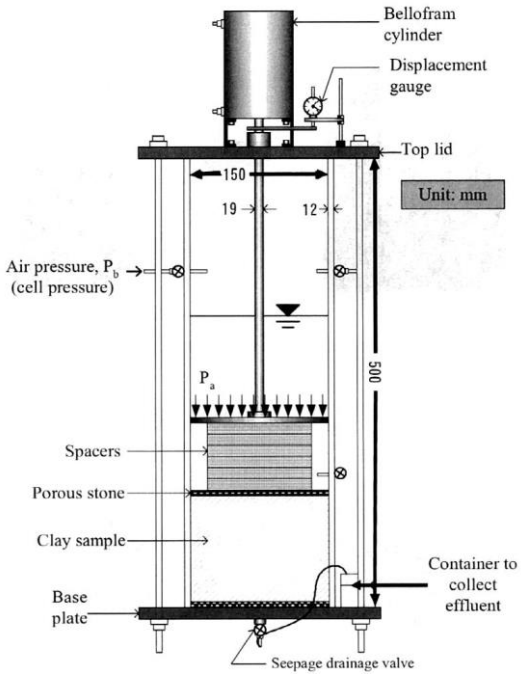

Fig. 2. 4 Schematic of column mold drawing for hydraulic conductivity test [8].

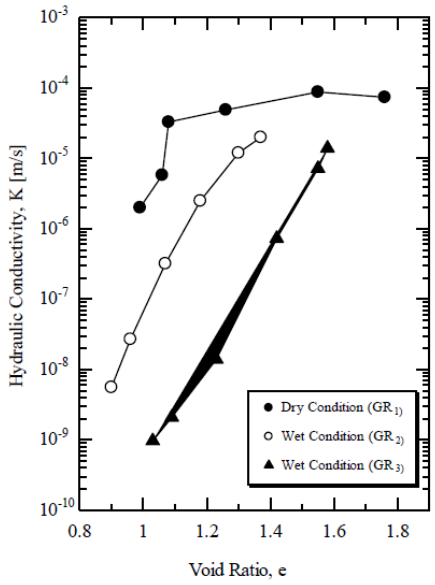

Fig. 2. 5 e-log K graph describes relation between hydraulic conductivity and void ration. As the pressure increased, the void ration (*e*) decreased and affected the decrease of *K* [7].

Even though bentonite has widely proved as an effective sorbent, however INB shows very low hydraulic conductivity $7x10^{-5}$ m/s – $2x10^{-6}$ m/s. The low of *K* value can be problem if INB is applied for bed sorbent. The seepage in the outlet will require long

time. Some previous researches developed clay composite with other material such as sand or other solid matrices that enhanced the permeability [9,10]. As mentioned in the research limitation, column sorption test in this research focused on the maximum sorption capacity improvement after milling modification. Further research to increase the hydraulic conductivity by composing milling modified INB with other solid matrices will be a crucial recommendation for scale-up application.

2.4.3 Swelling behavior effect

During unloading at 2 kPa in column mold *K* measurement of INB (water content initial=12.5%; water content final=36-43%), the lowering of *K* value by time was detected (Fig. 2.6, HC=hydraulic conductivity). The lowering *K* was observed in more than one month. Even though the lowering of *K* value was only small, however, this would be a crucial mechanism for predicting the long-term performance of *K* value. This *K* change seems to indicate the effect of swelling behavior due to water sorption into the void within the aggregate ($e_{aggregate}$) expanded which indicated by the increase of water content (w_c). As the water permeates to the aggregate of clay minerals, the spacing between particles of clay mineral began to compress due to the expansion of dielectric double layer (DDL) which makes water less mobile hence the *K* values decreased [7] (Fig.2.7).

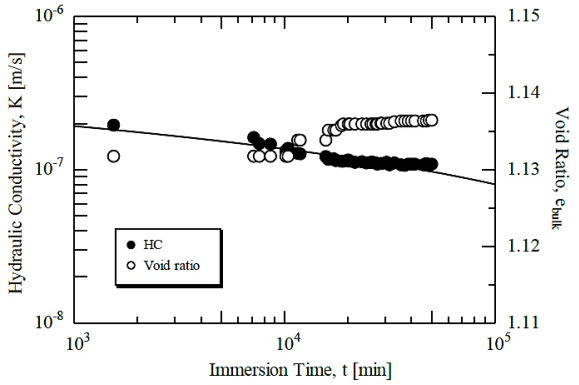

Fig. 2. 6 Lowering hydraulic conductivity during unloading at low-pressure 2kPa due to swelling in long-term measurement [7].

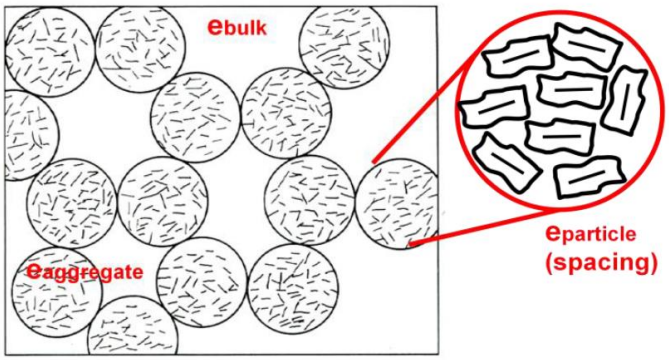

Fig. 2. 7 Schematic swelling mechanism [11].

References

[1] Indonesian Ministry of Energy and Mineral Resource, Book 3: Java Island, in: Indones. Geol. Resour., 2009.

[2] Badan Standarisasi Nasional, Klasifikasi Sumberdaya Mineral dan Cadangan, in: Standar Nas. Indones. Amandemen 1 - SNI 13-4726-1998 ICS 73.020, Badan Standarisasi Nasional - BSN, 1998.

[3] H. Pringgoprawiro, Biostratigrafi dan Paleogeografi Cekungan Jawa Timur Utara, Suatu Pendekatan Baru, Institut Teknologi Bandung, 1983.

[4] W. Prastistho, Geology and application of Wonosegoro, Boyolali Clay for Landfill Liner, Universitas Gadjah Mada, 2015.

[5] A. Yulianti, I.W. Warmada, A.D. Titisari, Characteristics and Genesis of Montmorilonitic Claystone From Bandung Area , Wonosegoro , Boyolali , Central Java , Indonesia, J. Southeast Asian Appl. Geol. 3 (2011) 64–71.

[6] C.E. Weaver, L.D. Pollard, Mixed-Layer Clay Minerals, in: Dev. Sedimentol., Elsevier Scientific Publishing Company, 1973: pp. 107–118. doi:https://doi.org/10.1016/S0070-4571(09)70011-1.

[7] M.A. Popang, Preliminary study of Kerek claystone properties and its application as a clayey barrier, Universitas Gadjah Mada, 2014.

[8] M.A. Tanchuling, J. Takemura, M.R.A. Khan, O. Kusukabe, Determination of Partitioning and Dispersion Coefficient Using Column Test, J. Southeast Asian Geotech. Soc. 37 (2006) 103–110.

[9] C.L. Ake, M.C. Wiles, H.J. Huebner, T.J. McDonald, D. Cosgriff, M.B. Richardson, K.C. Donnelly, T.D. Phillips, Porous organoclay composite for the sorption of polycyclic aromatic hydrocarbons and pentachlorophenol from groundwater, Chemosphere. 51 (2003) 835–844. doi:10.1016/S0045-

6535(03)00040-7.

[10] C.L. Ake, K. Mayura, H. Huebner, G.R. Bratton, T.D. Phillips, Development of porous clay-based composites for the sorption of lead from water, J. Toxicol. Environ. Health. 63 (2001) 459–475.

[11] J.K. Mitchell, Fundamentals of Soil Behavior, John Wiley & Sons, Inc., 1976.

CHAPTER 3
Characteristic change investigation of Indonesian natural bentonite during continuous milling

Morphological change, microstructural modification and deformation, change of specific surface area, microporosity, cation exchange capacity during, and particle size distribution during continuous ball-milling are presented and explained in detail in this chapter.

3.1 Sample preparation

The bentonite used was natural clay sampled from Wonosegoro area, Boyolali district, Central Java, Indonesia. The sample was air dried and crushed using mortar and sieved passed between 50 µm – 40 µm. One-gram sample was put into the jar and then milled using Retsch MM 400 with vibrational frequency 20 Hz for 2,5,10,15,20,25, and 30 minutes (Fig. 3.1). Lower vibrational frequency and shorter interval only yielded a negligible change of crystal structure. The mechanism of Retch MM is giving oscillating movement to the jar (Fig. 3.2). The metal ball inside the jar gives impact and friction to the sample inside (Fig. 3.2).

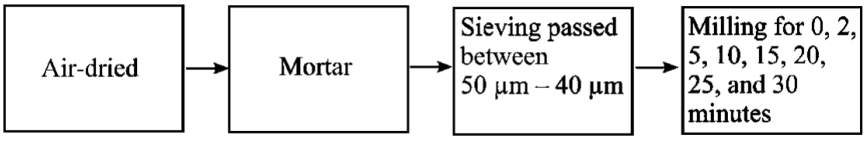

Fig. 3. 1 Schematic diagram of sample preparation

There was an increase of temperature during milling in jar. However, it was neglected since it did not affect the structure of montmorillonite. The first

change of montmorillonite due to temperature is at 100^{o} C which only dehydrates the water molecule in interlayer without changing the structure. Right after the milling finished, the jar was able to hold hand barely. Hence, it did not even reach 100^{o} C.

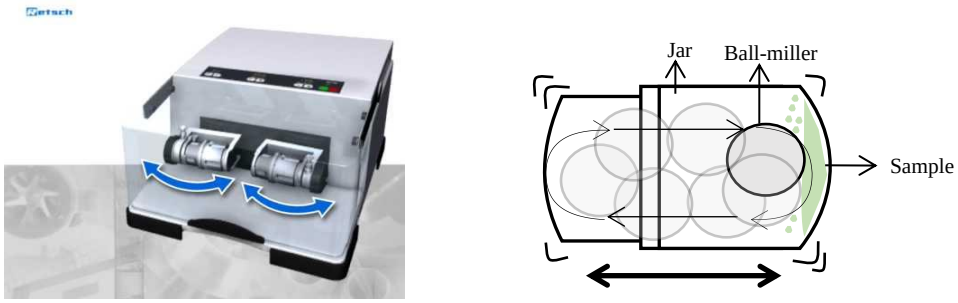

Fig. 3. 2 Ball miller Retsch MM 400 (left) and schematic of ball miller jar cross-section (right). The oscillating movement gives impact and friction on sample.

3.2 Instrumentation

Morphological changes before and after milling were observed using scanning electron microscope (SEM) Keyence VE-8800 with 5000 times magnifications. The structure of montmorillonite changes before and after milling was observed using x-ray diffraction (XRD) equipment Rigaku Multiflex with Cu source, operated at 40kV and 20 mA, measurement angle from 3^{o}-30^{o}. The surface functional group of montmorillonite before and after milling were recorded using Jasco FT/IR-6100FV Fourier Transform Infrared (FTIR) in the range of 400 - 4000 cm^{-1} (1 mg sample was mixed with 10 mg potassium bromide (KBr) and then pelletized). The CEC of samples were determined using Chapman method by saturating the samples with sodium acetate and then replaced the sodium with ammonium acetate [1]. Adsorption-desorption isotherm of the untreated and the mechanically deformed bentonites was measured using multiple-point nitrogen

adsorption-desorption technique, with BELSORP-max. Quantitative analysis of particle size was measured using SALD-2300 laser diffraction particle size analyzer.

3.3 Influence of progressive milling on morphology

The morphology of INB before milling and milling displayed in Fig. 3.3. The unmilled INB shows angular particles in aggregate. After 2 – 30 minutes milling, the morphology shows less aggregate angularity, more destructed and crumbled particles. Significant difference of surface texture is not found from 2 minutes to 30 minutes milling.

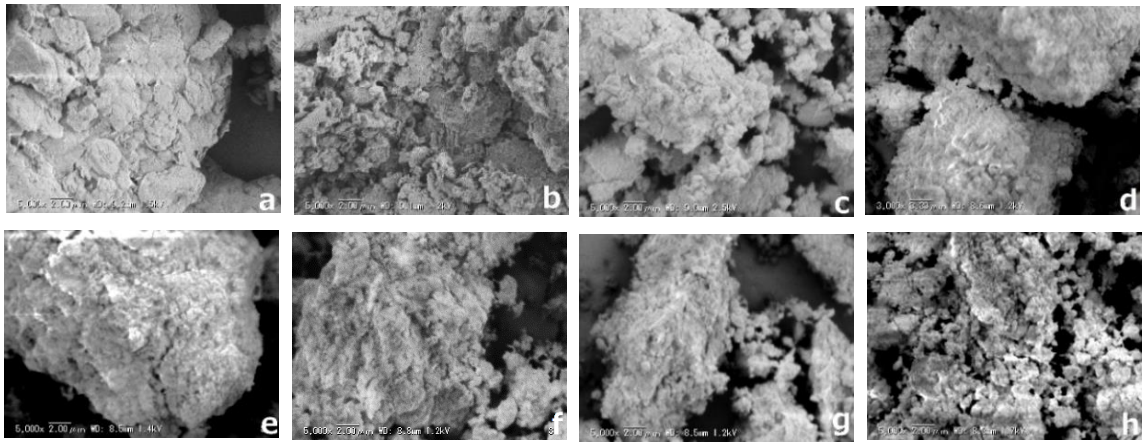

Fig. 3. 3 Morphology of unmilled (a) and milled bentonite: (b)2 minutes, (c)5 minutes, (d)10 minutes, (e)15 minutes, (f)20 minutes, (g)25 minutes, (h)30 minutes from SEM.

3.4 Influence of progressive milling on smectite structure

The influence of milling on montmorillonite structure can be seen in Fig. 3.4. Two minutes milling shows broadening line, decrease in intensity of montmorillonite (001) and basal spacing from 15.03 Å to 14.22 Å. The XRD pattern exhibits peak loss of montmorillonite (001) after 5 minutes milling but still retained the (100). The (100) montmorillonite peak intensity reduced after 10 minutes and could not be observed after 25 minutes milling.

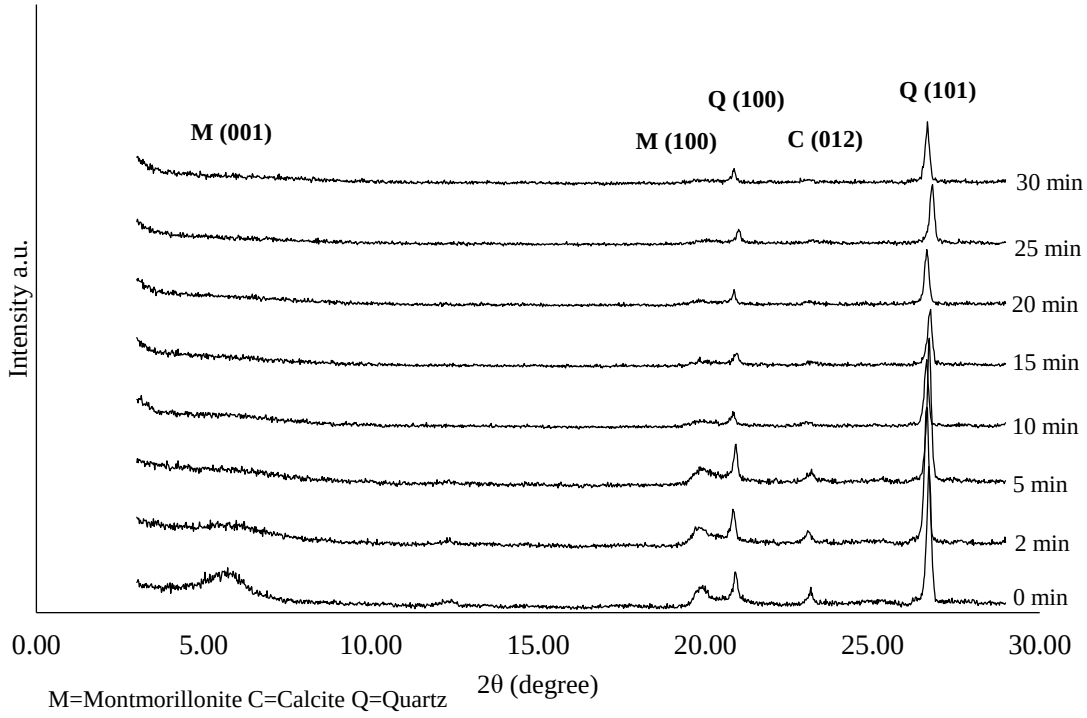

Fig. 3. 4 XRD pattern of unmilled and milled bentonite.

The changes in montmorillonite structure were also observed by FTIR (Fig. 3.5). The intensity of bands did not change for the unmilled sample, 2 minutes sample, and 5 minutes sample. The first change was noted from 10 minutes milled sample, 3621 cm^{-1} band (OH stretching) and 915 cm^{-1} (Al-Al-OH bending) which decrease in intensity, and loss peak for 854 cm^{-1} (Al-Mg-OH bending) (inset Fig. 3.6) [2–4]. The bands 915 cm^{-1} (Al-Al-OH bending) and 3621 cm^{-1} band (OH stretching) disappeared after 25 minutes milling (inset Fig. 3.7). The 529 cm^{-1} band (Al-O-Si bending) [3,5] decreased in intensity after 15 minutes milling and blunt after 25 minutes milling. The next intensity decrease was noted at 469 cm^{-1} band (Si-O-Si bending) [2,3] after 25 minutes milling. Slight band broadening was observed at 1031 cm^{-1} band (Si-O stretching) [3] after 25 minutes milling, and more broaden after 30 minutes milling (inset Fig. 3.8).

The CEC of unmilled and milled INB can be seen in Table 3.1. The unmilled INB shows very low of CEC compared to the other natural bentonites in general, 70 - 150

meq/100 gr [4,6–9]. However, one journal reported the CEC of natural bentonite near to INB location (around ±1 km to the south) only has 20 meq/100gr [10]. The natural bentonite in this area has low CEC. This cause can be explained if there are mixed-layer illite and montmorillonite which has CEC range 15-77 meq/100 gr [11]. The CEC was increased with the increase in milling time and reached a peak at 25 minutes milling and decreased after 30 minutes milling.

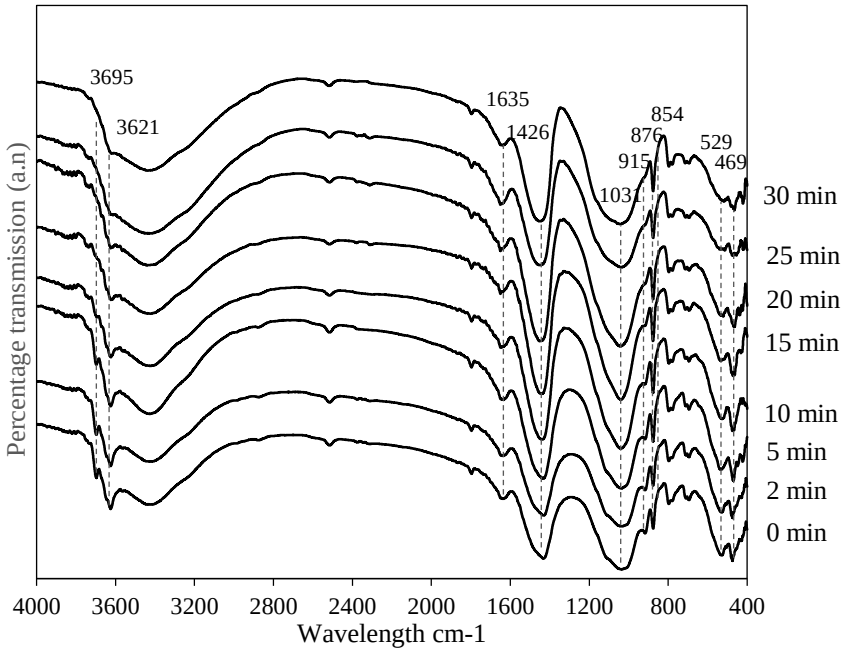

Fig. 3. 5 FTIR spectra of unmilled and milled INB.

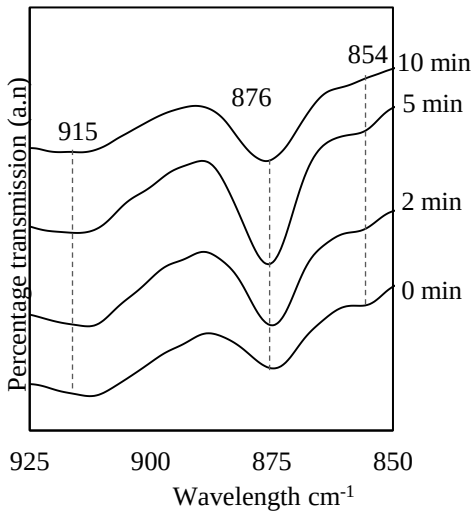

Fig. 3. 6 Inset of 854 cm^{-1} band (Al-Mg-OH) FTIR spectra which loss of peak after 10 minutes milling.

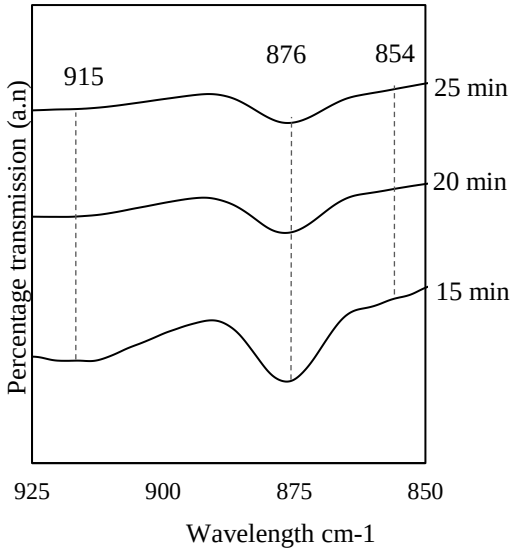

Fig. 3. 7 Inset of 915 cm^{-1} band (Al-Al-OH bending) FTIR spectra which loss of peak after 25 minutes milling.

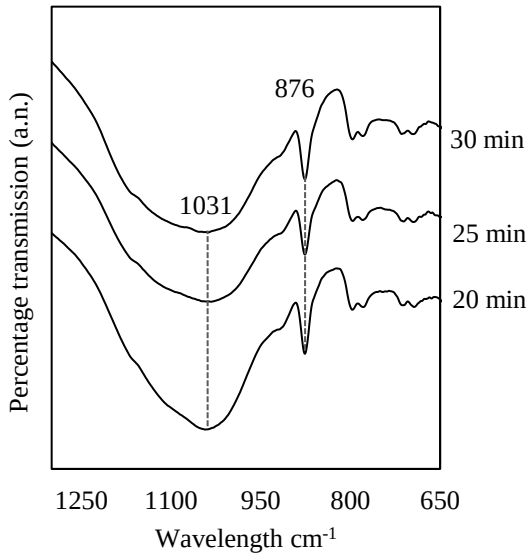

Fig. 3. 8 Inset of 1031 cm^{-1} band (Si-O-Si) FTIR spectra which slight broaden and decrease in intensity after 25 minutes milling.

3.5 Influence of progressive milling on SSA and microporosity

The adsorption-desorption of nitrogen are shown in Fig. 3.9. All of sample conditions exhibit hysteresis loops type H3 (IUPAC classification) which is typical for non-polar gas adsorption by natural montmorillonite [12]. The change of hysteresis loops

was observed from 5 minutes milling at which the magnitude of hysteresis is getting smaller in the end phase of milling.

Table 3.1 CEC of unmilled and milled INB

Milling time (minutes)	CEC (meq/100 gr)
0	17.54
2	20.04
5	22.79
10	32.22
15	33.42
20	34.63
25	35.39
30	33.08

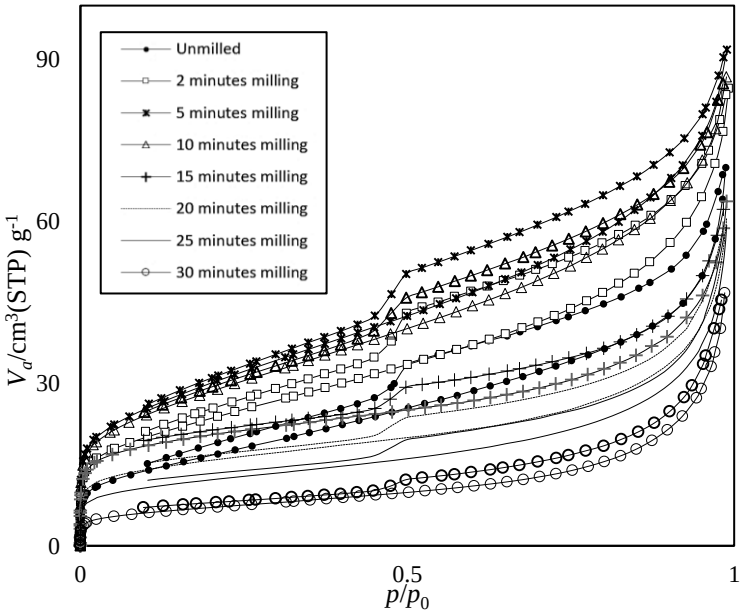

Fig. 3. 9 Adsorption-desorption isotherms of the original and milled bentonite

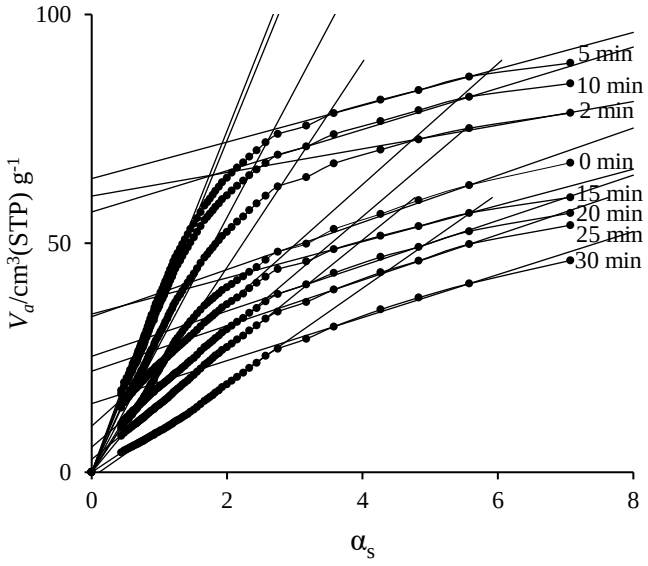

Fig. 3. 10 αs plot method

The SSA and microporosity parameter are listed in Table 3.2. The surface calculation was using Brunauer–Emmett–Teller (BET) method. The microporosity analysis was using α_s-plot method (Fig.3.10), which plot α_s as horizontal axis versus adsorbed amount where α_s:

$$\alpha_{s=}\frac{n_a}{n_{0.4}} \qquad (3.1)$$

n_a = adsorption amount at arbitrary equilibrium pressure

$n_{0.4}$ = adsorption amount at relative pressure p/p_0 = 0.4 of N_2 adsorption isotherm at 77 K of standard sample).

The slope and the intercept of the line in the middle mean mesopore/external surface area ($S_{m,e}$) and micropore volume (V_m). Meanwhile, the micropore surface (S_m) was obtained from $S_m = S_{BET} - S_{m.e}$.

Milling caused significant increase of SSA until 5 minutes milling but then gradually decreased for 10 to 30 minutes milling. The SSA values were even smaller than unmilled bentonite after 20 minutes milling. The change of micropore surface and

micropore volume pattern also consistent with the change of SSA which start the increase in micropore volume and then gradually decreased.

Table 3.2 Total SSA, external surface area, micropore surface and micropore volume of the unmilled and several minutes milled bentonite.

Milling time (minutes)	*SSA* (m^2/g)	$S_{m.e}$ (m^2/g)	S_m (m^2/g)	V_m (cm^3/g)
0	60.63	14.66	45.97	0.053
2	83.48	7.30	76.18	0.093
5	104.57	11.36	93.21	0.099
10	101.96	12.82	89.14	0.088
15	72.59	11.26	61.33	0.053
20	55.79	14.08	41.71	0.039
25	42.37	14.15	28.22	0.034
30	25.02	13.37	11.65	0.023

3.6 Influence of progressive milling on particle size distribution

The result from particle size distribution (PSD) measurement is shown in Fig. 3.11 and the mean of particle size values can be seen in Table 3.3. After 2 minutes milling, the mean of particle size reduced and increased after 5 – 10 minutes milling. Start from 10 minutes milling until 30 minutes milling the mean of particle sizes fluctuated.

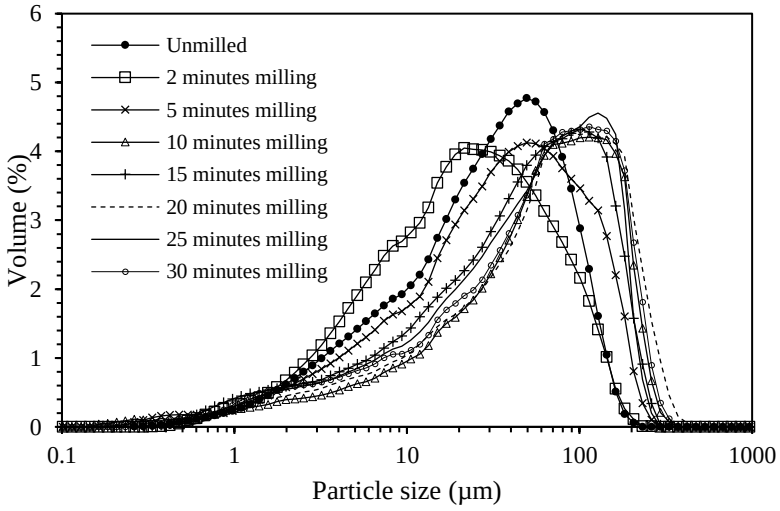

Fig. 3. 11 Particle size distribution of unmilled and milled INB.

Table 3.3 Mean particle size values of the unmilled and several minutes milling.

Milling time (minutes)	Mean particle size (μm)
0	49.28
2	21.43
5	49.28
10	113.34
15	100.63
20	113.42
25	127.67
30	113.34

3.7 Discussion

The XRD showed intensity and *d*-spacing decrease with broadening line after 2 minutes milling indicated the milling shifted the layer along the basal plane [13] and compressed it which affected the interlayer space became closer one another. The (001) montmorillonite disappeared after 5 minutes milling but still retained the (100) montmorillonite without significant intensity change after 5 minutes milling. This can be inferred that the montmorillonite layer was further shifted farther along the basal plane without destruction of montmorillonite layers. Moreover, since montmorillonite has a weak bond in interlayer, high frequency of retsch 400 MM ball miller type which applied impact and friction on sample, the montmorillonite was easily shifted along the basal plane and compressed. The FTIR spectra confirmed this, two OH bending groups in dioctahedral sheet: 854 cm^{-1} (Al-Mg-OH) and 915 cm^{-1} (Al-Al-OH) displayed unobservable intensity reduction from 0 minutes to 5 minutes milling (Fig. 3.5). After 10 minutes milling the XRD showed gradual intensity reduction of (100) montmorillonite peak, and finally, the peak disappeared after 25 minutes milling. The FTIR result also confirmed this by intensity loss of Al-Mg-OH bending and decrease of Al-Al-OH bending

after 10 minutes milling which followed by Al-O-Si bending decrease after 15 minutes milling, where Al is an octahedral cation [3]. Thus, the decrease in Al-O-Si bending indicates bond destruction between the tetrahedral and octahedral [2]. The destruction process of layer still noted from FTIR after 25 minutes milling. Si-O stretching and Si-O-Si bending which represents the group of tetrahedra [15,16] just started broadened at this point.

The SSA increased at the beginning of milling (2-5 minutes milling), in response to particle reduce and layer shifting which certainly opened new surfaces. An interesting finding in this study is the SSA started to decrease after 10 minutes milling but with the CEC still tended to increase. This can be explained if the swelling behavior of montmorillonite is taken into account. Even though the diameter of hydrated sodium is larger than nitrogen molecule [17,18], this hydrated cation expanded the interlayer of montmorillonite. The (001) montmorillonite was unobservable after milling. However, this swelling behavior could be observed on the unmilled sample after hydrated (Fig. 3.10). After 10 minutes milling, the narrowing interlayer no longer gave space for nitrogen molecule but still gave space for hydrated sodium. Another explanation is the consistent trend of micropore volume with SSA during the shifting condition is not acceptable if the interlayer is taken account into microporosity. The layer shifting should have reduced the micropore volume with the increase of SSA. The thickness of interlayer which only ~5 Å before milling and continuously narrower during milling time were not able to form multilayer of nitrogen in the interlayer. Hence, the nitrogen volume adsorbed in interlayer was counted as one side SSA at the time monolayer saturated condition in BET method. In this case, the micropore volume measured was between the edges of montmorillonite particles (interparticle microporosity) instead of in the interlayer. Schematic illustration depicted in Fig. 3.11. Another author also noted similarities to this.

The SSA determination by BET method using N_2 physisorption did not exactly represent the surface area but also included microporosity [19]. Another cause of SSA decrease that can be inferred as well is gradually broken of octahedral sheet after 10 minutes and contributed shortening of the *bc* plane of montmorillonite.

The cause of CEC increase in the beginning phase was similar to SSA, particle size reduction, and layer shifting. After 10 minutes milling, the increase was in response to gradual octahedral layer destruction. The Al-Mg-OH collapse which followed by Al-Al-OH, raised the negative charge of layer. After reaching the peak at 25 minutes milling, the CEC decreased due to the amorphization of tetrahedral sheet and also the enclosed of interlayer. The later reason, however it based on the decreasing trend of the basal spacing from XRD pattern before the (001) ruptured.

Particle size distribution showed the particle size of unmilled and milled INB are >4 µm. According to the Udden-Wenworth scale classification, this means the particle size analyzer equipment still measured the clay in aggregate not the particle of clay. The result showed aggregate reduced after 2 minutes milling and reaggregated from 5 minutes milling until 10 minutes milling. The reaggregation stopped from 10 minutes milling until 30 minutes milling by showing repetitive disaggregation – reaggregation. The disaggregation and reaggregation did not affect the increase and the decrease of SSA. Hence, this is contrary to the previous study (mentioned in chapter 1). Agglomeration did not represent the clogging of mineral surfaces which caused the decrease of SSA.

The relationship between CEC, SSA, microporosity, and particle size distribution change during progressive milling time is summarized in this graph illustration (Fig. 3.12). A slight moment during amorphization of montmorillonite was found which brought the optimum value of CEC before it tended to decrease. The destruction of octahedral sheet before the tetrahedral sheet amorphization due to progressive ball milling

did bring benefit instead. The increase was in response to the loss of cation in the octahedral sheet which affected to higher negative charge.

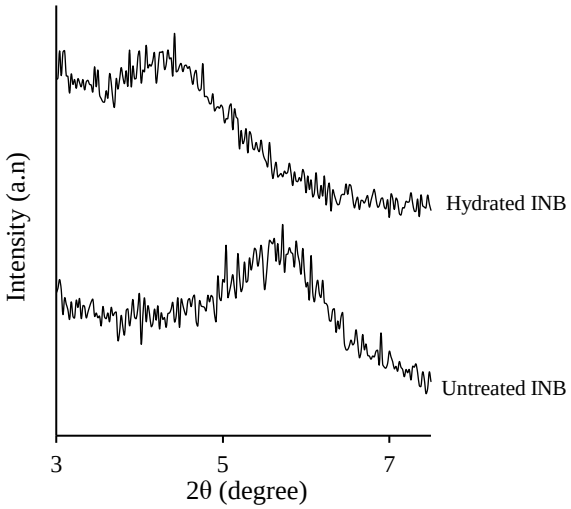

Fig. 3. 12 Increasing basal spacing (001) montmorillonite from 15.04 Å to 19.9 Å of INB after hydrated indicated swelling behavior.

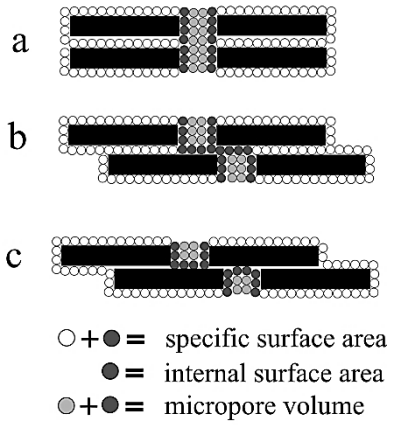

Fig. 3. 13 Schematic of SSA decrease due ball milling: a) The unmilled condition, b) 2-5 minutes milling which opened new surface and tighter interlayer but still could accommodate nitrogen molecule, c) 10 minutes milling, the interlayer no longer accommodated space for nitrogen molecule and the octahedral layer started to collapse which caused SSA decreased.

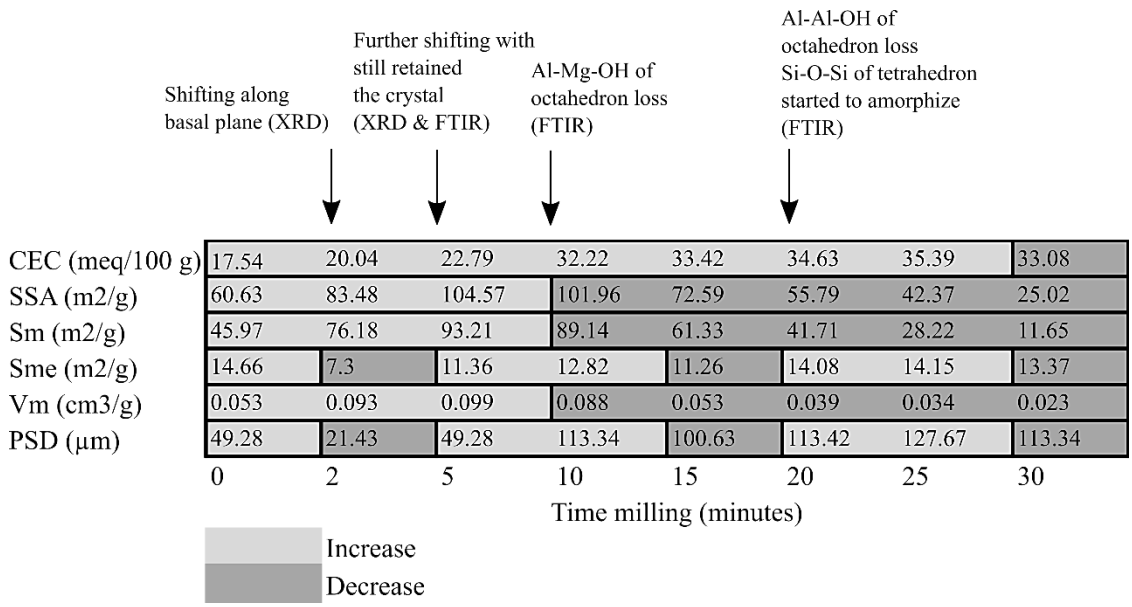

Fig. 3. 14 Relationship of all characterizations during progressive milling on INB

3.8 Summary

The following are some important points discussed in this chapter:

- The (001) intensity decreased and broadened after 2 minutes milling, and loss after 5 minutes milling did not show montmorillonite amorphization and destruction. The amorphization of montmorillonite was able to be observed from the (100) which started after 10 minutes milling.
- The montmorillonite structure amorphization and destruction were noted in detail from the FTIR. Peak loss of Al-Mg-OH of octahedral sheet showed after 10 minutes milling which indicated destruction. The destruction of Al-Mg-OH then followed by the Al-Al-OH of octahedral sheet at 25 minutes milling. Slight peak reduced and broadened of Si-O of tetrahedron noted at 25 minutes milling and continued at 30 minutes milling.
- The CEC increased with the increase of milling time and reached the peak after 25 minutes milling and started to decrease after 30 minutes milling.

- The SSA and microporosity tended to increase until 5 minutes milling and decrease from 10 minutes milling.
- The particle size distribution decreased at 2 minutes milling, reaggregated from 5 minutes milling, and stop reaggregating from 10 minutes milling.

References

[1] H.D. Chapman, “Cation Exchange Capacity,” In: C.A. Black, Ed., Methods of Soil Analysis-Chemical and Microbiological Properties, 9 (1965) 891–901.

[2] J. Hrachová, P. Komadel, V.Š. Fajnor, The effect of mechanical treatment on the structure of montmorillonite, Mater. Lett. 61 (2007) 3361–3365. doi:10.1016/j.matlet.2006.11.063.

[3] M. Hayati-Ashtiani, Use of FTIR spectroscopy in the characterization of natural and treated nanostructured bentonites (montmorillonites), Part. Sci. Technol. 30 (2012) 553–564. doi:10.1080/02726351.2011.615895.

[4] G.E. Christidis, F. Dellisanti, G. Valdre, P. Makri, Structural modifications of smectites mechanically deformed under controlled conditions, Clay Miner. 40 (2005) 511–522. doi:10.1180/0009855054040188.

[5] E. Srasra, F. Bergaya, J.J. Fripiat, Infrared spectroscopy study of tetrahedral and octahedral substitutions in an interstratified illite-smectite clay, Clays Clay Miner. 42 (1994) 237–241. doi:10.1346/CCMN.1994.0420301.

[6] A. Djukić, U. Jovanović, T. Tuvić, V. Andrić, J. Grbović Novaković, N. Ivanović, L. Matović, The potential of ball-milled Serbian natural clay for removal of heavy metal contaminants from wastewaters: Simultaneous sorption of Ni, Cr, Cd and Pb ions, Ceram. Int. 39 (2013) 7173–7178. doi:10.1016/j.ceramint.2013.02.061.

[7] N. Vdovic, I. Jurina, S.D. Škapin, I. Sondi, The surface properties of clay minerals modified by intensive dry milling - revisited, Appl. Clay Sci. 48 (2010) 575–580. doi:10.1016/j.clay.2010.03.006.

[8] N. Stanković, M. Logar, J. Luković, J. Pantić, M. Miljević, B. Babić, A. Radosavljević-mihajlović, Characterization of bentonite clay from “ Greda ” deposit, Process. Appl. Ceram. 5 (2011) 97–101. doi:10.2298/PAC1102097S.

[9] E. Busenberg, C. V. Clemency, Determination of the cation exchange capacity of clays and soils using an ammonia electrode, Clays Clay Miner. 21 (1973) 213–217. doi:10.1346/CCMN.1973.0210403.

[10] A. Yulianti, I.W. Warmada, A.D. Titisari, Characteristics and Genesis of Montmorilonitic Claystone From Bandung Area , Wonosegoro , Boyolali , Central Java , Indonesia, J. Southeast Asian Appl. Geol. 3 (2011) 64–71.

[11] C.E. Weaver, L.D. Pollard, Mixed-Layer Clay Minerals, in: Dev. Sedimentol., Elsevier Scientific Publishing Company, 1973: pp. 107–118. doi:https://doi.org/10.1016/S0070-4571(09)70011-1.

[12] R.M. Barrer, Clay minerals as selective and shape-selective sorbents, Pure Appl. Chem. 61 (1989) 1903–1912. doi:10.1351/pac198961111903.

[13] I. Sondi, M. Stubičar, V. Pravdić, Surface properties of ripidolite and beidellite clays modified by high- energy ball milling, Colloids Surfaces A Physicochem. Eng. Asp. 127 (1997) 141–149. doi:10.1016/S0927-7757(96)03893-9.

[14] V.. Farmer, The layers silicates, in: Infrared Spectra Miner., Mineralogical Society, London, 1974: pp. 331–363. https://doi.org/10.1180/mono-4.

[15] B. Čičel, G. Kranz, Mechanism of Montmorillonite Structure Degradation by Percussive Grinding, Clay Miner. 16 (1981) 151–162. doi:10.1180/claymin.1981.016.2.03.

[16] B. Tyagi, C.D. Chudasama, R. V. Jasra, Determination of structural modification in acid activated montmorillonite clay by FT-IR spectroscopy, Spectrochim. Acta - Part A Mol. Biomol. Spectrosc. 64 (2006) 273–278. doi:10.1016/j.saa.2005.07.018.

[17] C.G. Schull, The Determination of Pore Size Distribution from Gas Adsorption Data, J. Am. Chem. Soc. 70 (1948) 1405–1410. doi:10.1021/ja01184a034.

[18] Y. Marcus, Ionic Radii in Aqueous Solutions, Chem. Rev. 88 (1988) 1475–1498. doi:10.1021/cr00090a003.

[19] S. Kaufhold, R. Dohrmann, M. Klinkenberg, S. Siegesmund, K. Ufer, N2-BET specific surface area of bentonites, J. Colloid Interface Sci. 349 (2010) 275–282. doi:10.1016/j.jcis.2010.05.018.

CHAPTER 4
Batch sorption test

The effect of ball-milling on Indonesian natural bentonite (INB) for Mn sorption is elucidated through batch sorption test effect of contact time. The highest sorption capacity is selected for the next experiments: effect of different sorbate concentration and effect of different pH. Mathematical model the Langmuir and Brunauer, Emmet, and Teller (BET) model are also described.

4.1 Sample preparation

Similar sample preparation as in chapter 3 was conducted. In the batch sorption study, the samples chosen for the effect of contact time experiment are the unmilled, 10 minutes milling (when the octahedral layer lost its cation Mg^{2+}), 25 minutes milling (when the octahedral sheet lost its cation Al^{3+}, INB reached the highest CEC, and the tetrahedral sheet started to have slight amorphization), and 30 minutes milling (when the further amorphization of tetrahedral sheet occurred and CEC started to decrease). Comparison with Wako industrial bentonite was also included. Meanwhile, for the effect of sorbate concentration, effect of pH, and fitting model study would be comparison between the unmilled and the highest sorption capacity from the effect of time experiment result.

4.2 Instrumentation

The concentration of all sample solutions taken was measured using induced coupled plasma atomic emission spectroscopy (ICP-AES) Seiko Instrument, SPS 7800 (II).

4.3 Batch sorption study

4.3.1 Effect of contact time

50 ml aliquots with 24 mg/L of manganese solution (diluted from Mn $(NO_3)_2$ Wako standard solution 1000 ppm) was prepared into five 50 ml beaker glasses. The pH was 2.8. Unmilled and milled INB samples with mass 0.1 g were added to each beaker glass. Magnetic stirrer was used to mix the sample and solution. The stirrer was set 320 rotations per minute (RPM) at room temperature. The sample was taken from the mixture at 10 min, 20 min, 30 min, 1 h, 2 h, 4 h, 6 h, and 8 h. The Mn sorbed on INB then calculated using equation 1.3.

The effect of contact time on the sorption of manganese was shown in Fig. 4.1. It shows after milling the sorption capacity increases significantly and reaches the highest at 25 minutes milling. The increase of sorption capacity even better than Wako bentonite. The sorption rate of samples initially increased rapidly and reached the equilibrium in 2 hours with pH ~8. Based on this result the unmilled and 25 min milled (the highest sorption capacity) INB are chosen for the next experiment

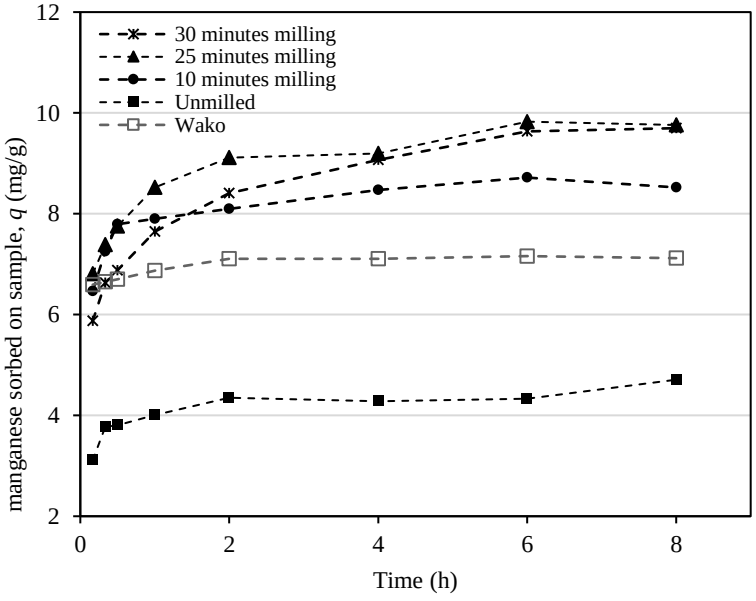

Fig. 4. 1 Effect of contact time of manganese sorption

4.3.2 Effect of sorbate concentration

Five different concentration of manganese solutions were prepared (diluted from Mn $(NO_3)_2$ Wako standard solution 1000 ppm): 6.5, 13.1, 24, 43.3, and 83 mg/L with volume 50 mL of each concentration. Each concentration was prepared in two portions. The unmilled and the highest sorption capacity from the effect of contact time experiment, which is 25 minutes milled INB sample were selected. Mass of 0.1 g of unmilled and 25 minutes milled sample was added into each solution prepared. The stirrer was also set 320 RPM at room temperature until equilibrium condition.

Variation of Mn removal in various concentration is shown in Fig. 4.2. As the Mn concentrations increased, the percentage removal decreased. When the Mn concentration is low, more surfaces the Mn is attached. In contrary, the surfaces become fewer when the concentration is high.

Milled INB shows an increase in removal percentage compared to the unmilled around 27-40%.

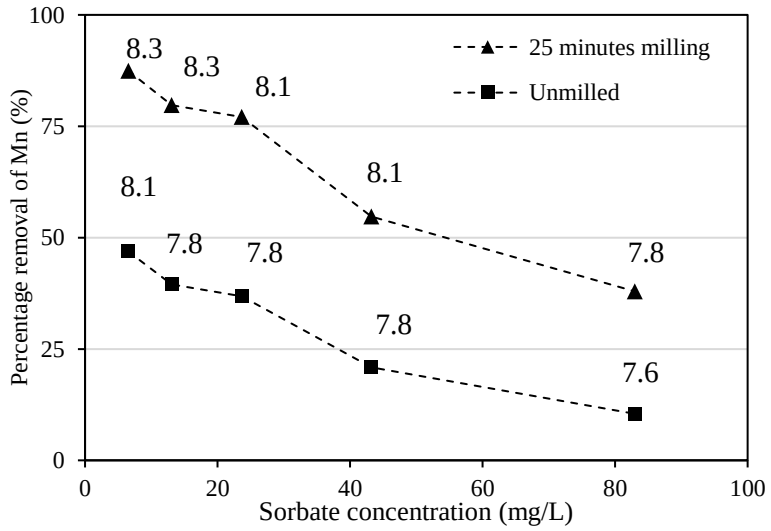

Fig. 4. 2 Effect of Mn concentration with values above the point exhibits pH equilibrium.

4.3.3 Effect of different pH

Five different pH of 24 mg/L manganese solutions were prepared (diluted from Mn $(NO_3)_2$ Wako standard solution 1000 ppm): 2.8, 3.9, 5.1, 6.7, and 7.9 with volume 50 mL of each. Each pH was prepared in two portions. 0.1 g of unmilled and 25 minutes milled sample was added each of it. The stirrer was also set 320 RPM at room temperature until equilibrium condition.

The effect of different pH on Mn sorption from solution is shown in Fig. 4.3. It can be observed that the sorption of Mn increases with the increase of pH in the solutions. Bentonite, which dominantly contains smectite mineral is known to possess negative surface charge due to isomorphic substitution in octahedral layer [1,2]. The change of pH will also change the surface charge of smectite. In lower pH, protonation on tetrahedral layer surface of smectite tends to intense which cause the decrease in surface charge. Hence, lower pH causes lesser Mn sorbed on bentonite, and higher pH will affect more Mn sorbed.

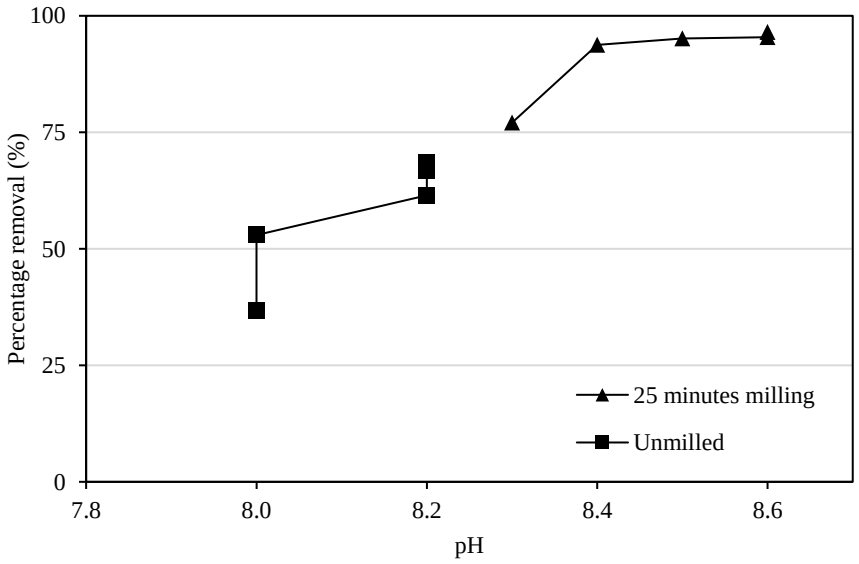

Fig. 4. 3 Effect of different pH of Mn sorption at equilibrium condition.

4.3.4 Fitting model

In order to get the Langmuir constant k and Q_m (maximum sorbate sorbed on sorbent) the equation (1.3) is linearized into this equation:

$$\frac{C_e}{q_e} = \frac{1}{Q_m k_L} + \frac{C_e}{Q_m} \tag{4.1}$$

where, C_e = equilibrium concentration (mg/L), q_e = amount of sorbate sorbed on sorbent at equilibrium, Q_m = maximum sorbate sorbed on sorbent (mg/g), and k_L = Langmuir constant.

The BET model is formulated in eq. 1.5 and can be linearized as follows:

$$\frac{C_e}{[qe(C - C_e)]} = \frac{\left[1 + (k_B - 1)\frac{C_e}{C}\right]}{Q_m k_B} \tag{4.2}$$

The Langmuir and BET plot of unmilled and milled INB can be seen in Fig. 4.4 and Fig. 4.5, and the parameter can be seen in Table 4.1. Table 4.1 shows that the sorption data fitted well to Langmuir isotherms than the BET. The correlation coefficient of both unmilled and milled sample shows 0.99. The maximum Mn sorbed on INB sample shows significant improvement almost four times after 25 minutes milling.

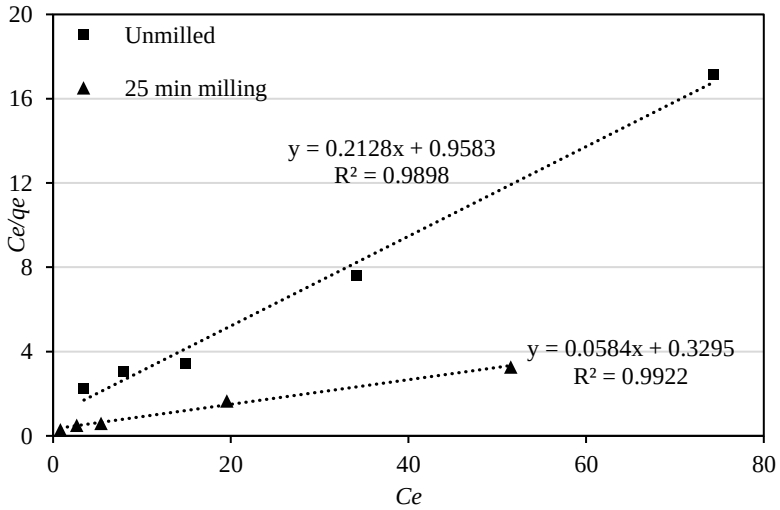

Fig. 4. 4 Linearized Langmuir plot model.

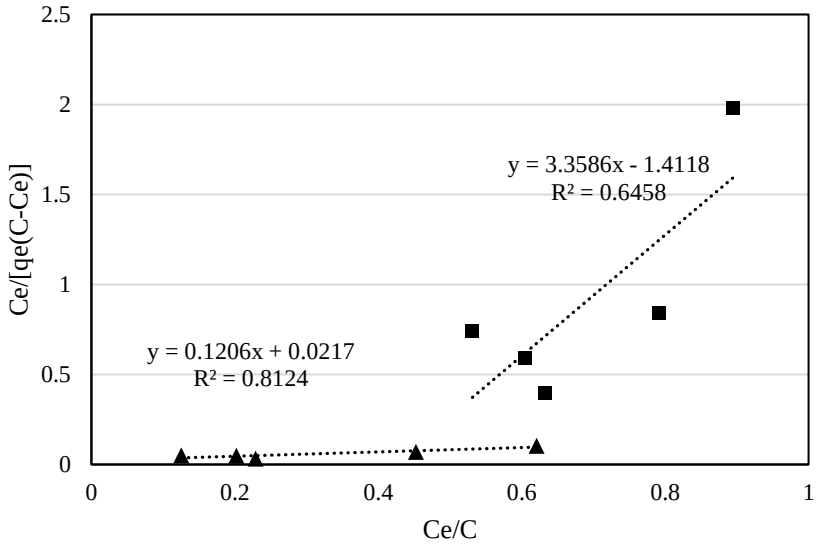

Fig. 4. 5 Linearized BET plot model.

Table 4.1. Parameters of Langmuir and BET

Time milling	Langmuir			BET		
	R^2	Q_m (mg/g)	k (L/mg)	R^2	Q_m (mg/g)	k
0 min	0.99	4.69	0.22	0.64	1.18	-3.74
25 min	0.99	17.12	0.17	0.81	45.96	1.00

4.4 Discussion

The Mn uptake on INB reached the best performance at 25 minutes milling. This meets agreement with the maximum CEC described in chapter 3. The increase of negative charge of montmorillonite was affected by the disappearance of cation in the octahedral sheet. In consequence, the surface attracted more Mn cation to satisfy the deficiencies. Similar with the decreasing trend of CEC, further amorphization on tetrahedral layer surface at 30 minutes milling caused Mn uptake became decrease.

The interesting finding in this investigation is an increase of R^2 in BET isotherm after milling. Ca-bentonite is known to have a diffuse double layer on the outer surface

of tactoids of montmorillonite mineral while in internal surface or interlayer only forms monolayer cations without diffuse double layer [3]. Previous studies described milling had affected clay mineral shifting along the basal plane [4–6]. In this study allegedly, there was a development of secondary active sites on INB after milling due to the shifting of montmorillonite array. This shifting yielded more new surfaces to formed new diffuse double layer attaching the Mn cations. The higher R^2 of the BET isotherms after milling is probably indicated the development of multilayer sorption in response to the development of diffuse double layer. On the other hand, the increase of negative surface charge due to cation destruction in the octahedral sheet could also attract more Mn concentration in diffuse double layer.

4.5 Summary

The following are some important points discussed in this chapter:

- Progressive milling on INB showed the highest sorption capacity at 25 minutes milling.
- In various of Mn concentration, the percentage of Mn uptake decreased as the Mn concentration increased.
- In various pH values, the percentage of Mn uptake decreased as the pH in the lower value.
- The Langmuir model is more suitable than the BET as the R^2 of Langmuir closer to 1.

References

[1] R.E. Grim, Clay Mineralogy, McGraw Hill Book Company, 1968.

[2] M.E. Essington, Soil and Water Chemistry: An integrative approach, CRC Press, 2004. doi:10.1017/CBO9781107415324.004.

[3] A.V. Blackmore, R.D. Miller, Tactoid size and osmotic swelling in calcium montmorillonite, Soil Sci. Soc. Am. J. 25 (1960) 169–173.

[4] W. Prastistho, W. Kurniawan, H. Hinode, Ball-milling effect on Indonesian natural bentonite for manganese removal from acid mine drainage, in: MATEC Web Conf., 2018: pp. 1–5. doi:10.1051/matecconf/201815603046.

[5] I. Sondi, M. Stubičar, V. Pravdić, Surface properties of ripidolite and beidellite clays modified by high- energy ball milling, Colloids Surfaces A Physicochem. Eng. Asp. 127 (1997) 141–149. doi:10.1016/S0927-7757(96)03893-9.

[6] N. Vdovic, I. Jurina, S.D. Škapin, I. Sondi, The surface properties of clay minerals modified by intensive dry milling - revisited, Appl. Clay Sci. 48 (2010) 575–580. doi:10.1016/j.clay.2010.03.006.

CHAPTER 5
Column sorption test

Application of optimized milled Indonesian natural bentonite (INB) on fixed-bed column sorption is presented in this chapter. Mass transfer zone (*MTZ*), length of unused bed (*LUB*), and mathematical model of Thomas, Adams-Bohart, and Yoon-Nelson are explained. The explanation presents comparison between unmilled INB and after milling modification.

5.1 Sample preparation and experiment

1. Unmilled and effective milled INB (25 minutes milling on INB) are prepared in the cartridge column (Fig. 5.1).
2. The vacuum chamber has 10 slots, 5 in the front and 5 in the back with container glass inside. The cartridge column with the INB sample inside was set on the valve.
3. Before feeding the column by manganese solution, the column was fed using distilled water until the sample saturated.
4. A Vacuum pump was applied in the vacuum chamber which took up the solution from the bottom of cartridge column.
5. The water remained in the column above sample was disposed.
6. To clean the water remained in the sample, the vacuum pressure was applied for around 1 minute.
7. The manganese solution with concentration 2.4 mg/L, pH 2,8 (referred to the AMD coal mining company in Jorong area, South Kalimantan, Indonesia [1]) was poured to the cartridge until 5.5 cm in height counted from the bottom of the sample and kept in constant during the experiment.
8. The vacuum pressure was then turned on. The initial flow rate for the unmilled INB was 0.04 Mpa and for the milled INB was 0.01 Mpa. These values were known by several trials before this experiment to obtain the same flow rate 0.8 mL/min.

9. The valve was opened and the time started to be accounted using a stopwatch.
10. Right the time the manganese solution reached 5 mL inside the container glass, the valve was then closed, and the stopwatch was paused and the time was recorded. The cartridge column was then quickly moved to the next slot and done the similar way as before.
11. When all the containers are full, immediately the containers were replaced by the empty and started again as number 8. The effluent samples are filtered and put into the sample bottle.
12. The concentration of all samples is measured using induced coupled plasma atomic emission spectroscopy (ICP-AES) Seiko Instrument, SPS 7800 (II).

The specifications that used in calculation described as belows:

Column diameter (D) = 1.6 cm

Cross sectional area of column (A) = 2.01 cm^2

Sample mass (m) = 0.5 g

Average flow rate (F) = 0.8 mL/min

Linear velocity (F/A) = 0.4 cm/min

Bed height (Ht) = 0.3 cm

Initial concentration of Mn (Co) = 24 mg/L, pH=2.8

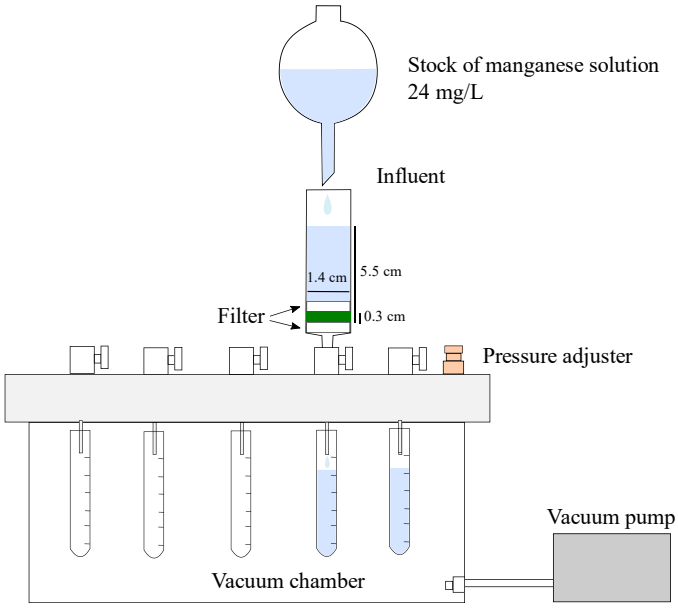

Fig. 5. 1 Schematic diagram of column sorption setup

During the operation the initial pressure of the unmilled was set -0.04 Mpa to obtain flow rate 0.8 mL/min. The pressure was gradually adjusted to the lower value and reached steady in around 30 minutes with -0.025 Mpa. After 30 minutes, only a little pressure adjustment upper and lower required to keep the flow rate constant. The initial pressure of the milled INB was set -0.01 Mpa to obtain the same flow rate with the pressure gradually also adjusted to the lower value and reach steady in around 20 minutes with -0.005 Mpa. The little adjustment also conducted to keep the flow rate constant. The constancy of flow rate is shown in Fig. 5.2 and Fig. 5.3 by plotting the time and volume.

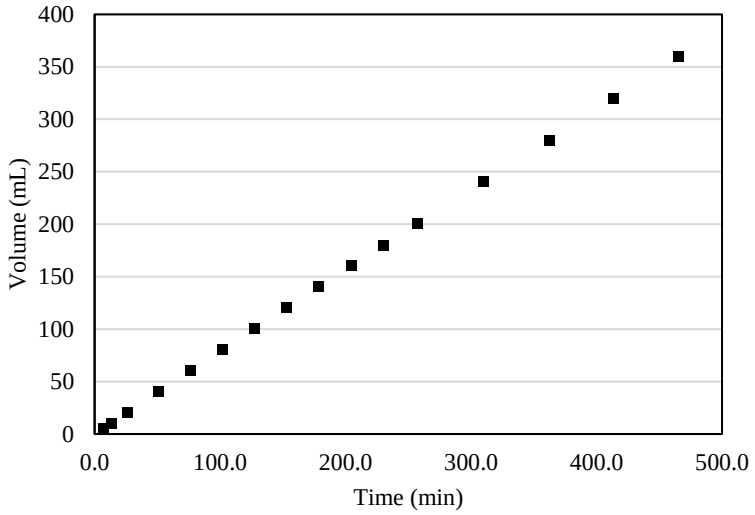

Fig. 5. 2 Constant flow rate showed by linear line (unmilled INB)

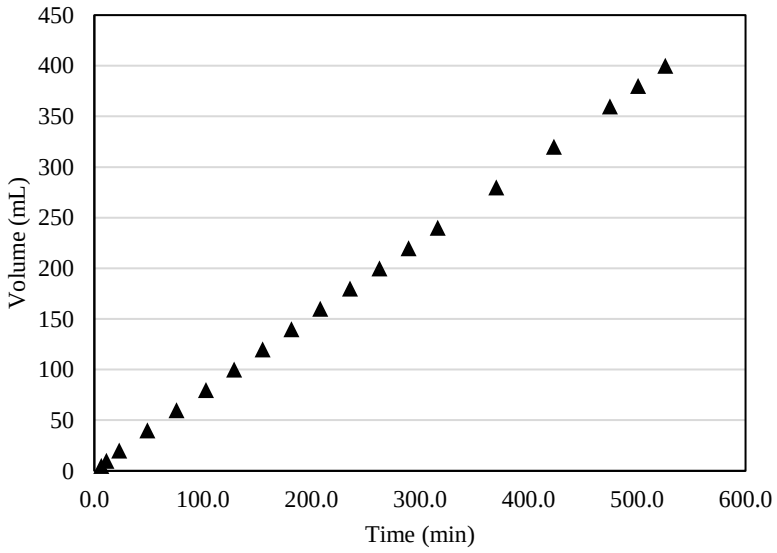

Fig. 5. 3 Constant flow rate showed by linear line (milled INB)

In this operation, the breakthrough time was set at concentration in effluent reached 4 mg/L (C/Co 0.17), referring to Indonesian government regulation of the maximum limit of Mn concentration for mining waste [2]. Fig. 5.4 shows breakthrough curves of unmilled and 25 min milled INB. In same flow rate, bed length, and initial concentration of the influent solution, unmilled INB reaches breakthrough time (*tb*)faster than milled INB. The breakthrough times are 37 minutes for the unmilled and 277 minutes for the milled INB. This indicates milled INB sorbed Mn more than the unmilled. The volume of remediated until *tb* time are recorded 35 mL for unmilled INB and 205 mL for milled INB (Fig. 5.5).

The pH of effluent from both unmilled and milled INB was measured at the first time come out from the outlet at around 6 minutes, during breakthrough, and when reached equilibrium. Both unmilled and milled showed pH 8 in three conditions above.

The amount of metal sorbed until t_b and until saturation time (*sat*) is expressed in eq. (5.1) (q_u) and eq. (5.2) (q) as follows:

$$q_u = \frac{C_0 F}{m} \int_0^{t_b} \left(1 - \frac{C}{C_0}\right) dt \tag{5.1}$$

$$q = \frac{C_0 F}{m} \int_0^{\infty} \left(1 - \frac{C}{C_0}\right) dt \tag{5.2}$$

where, C_0 = initial concentration (mg/L), F = flow rate (mL/min), m = mass of sorbent (g). The calculation of mass transfer zone length (*MTZ*) used simplified equation (eq. (5.3)) introduced by Geankoplis (1993) [3].

$$MTZ = \left(1 - \frac{q_u}{q}\right) Ht \tag{5.3}$$

where *Ht* = total height of (cm). The length of unused bed (*LUB*) was calculated using equation (eq. (5.4)) as follows:

$$\frac{LUB}{L_T} = 1 - \frac{t_b}{t^*} \tag{5.4}$$

where, LT = length of bed (cm), t^* = stoichiometric time (min) at the midpoint of breakthrough curve which is the ideal time for breakthrough.

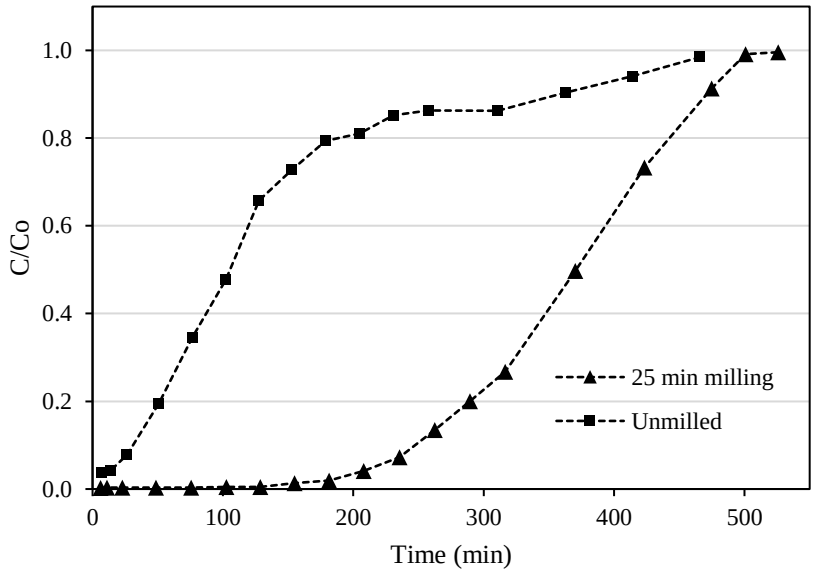

Fig. 5. 4 Breakthrough curves of unmilled and 25 minutes milled INB time versus C/Co

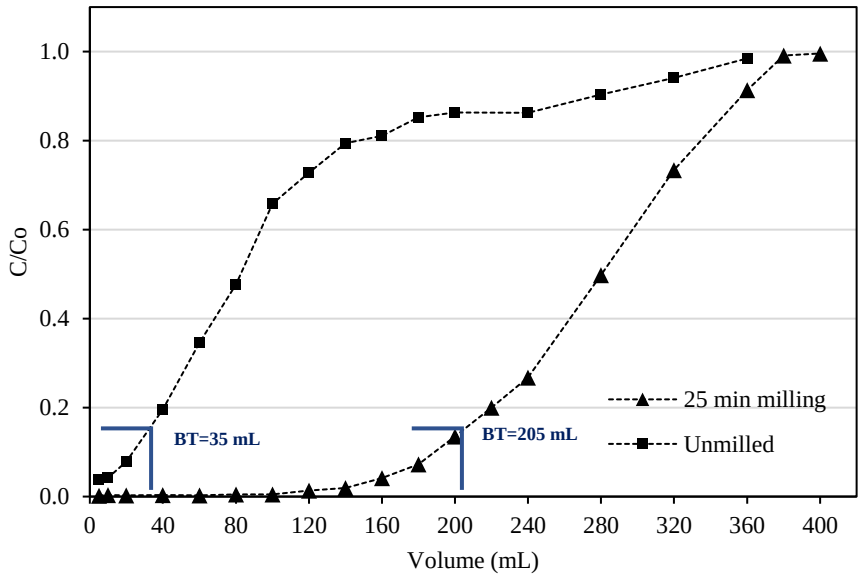

Fig. 5. 5 Breakthrough curves of unmilled and 25 minutes milled INB time versus C/Co

All of the breakthrough parameter calculation results are presented in Table 5.1.

The milled INB exhibits higher value for Mn removal. The length of *MTZ*, or equivalently, the difference between breakthrough and saturated time, exhibit significantly smaller after 25 minutes milling. In the same condition of flow rate, influent concentration, and bed length, smaller *MTZ* would give longer breakthrough time.

Table 5.1 Parameters of breakthrough curves

Sample	*qu* (mg/g)	*q* (mg/g)	*t** (min)	*MTZ* (cm)	*LUB* (cm)
Unmilled	1.27	4.55	200	0.22	0.24
Milled	10.06	12.91	375	0.07	0.08

5.2 Bed model

Bed model aims to select an analytical solution that describes and predicts the behavior of the breakthrough curves of Mn removal by unmilled and milled INB in fixed bed. In sorption column process, the knowledge of breakthrough curve prediction and its parameters behavior are important to obtain optimal successful design.

The Thomas equation is expressed in eq. 1.6 and can be linearized as follows (eq. (5.5)):

$$\ln\left(\frac{C_0}{C_t}-1\right)=\frac{k_{Th}q_0m}{v}-k_{Th}C_0t \tag{5.5}$$

where, k_{Th} = Thomas rate constant (L/min.mg), q_0 = equilibrium uptake of sorbate (mg/g), m = mass of sorbent (g), C_0 = influent concentration (mg/L), C_t = effluent concentration at time (t) (min), v = flow rate (mL/min) (the values mentioned in section 5.1). Linier regression analysis for breakthrough curve using Thomas model is depicted in Fig. 5.6.

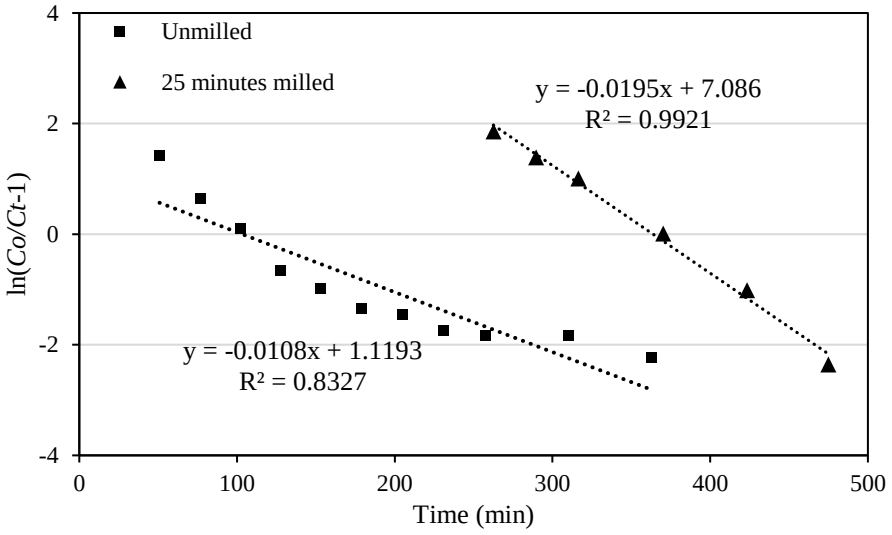

Fig. 5. 6 Thomas model linear regression

The Adams-Bohart equation is expressed in eq.1.8 and linearized as follows (eq. (5.6)):

$$\ln \frac{C_t}{C_0} = k_{AB} C_0 t - k_{AB} N_0 \frac{H}{U_0} \tag{5.6}$$

where, k_{AB} = kinetic constant (L/mg.min), N_0 = saturation concentration (mg/L), U_0 = linier velocity (cm/min), H = depth of bed (cm) (the values mentioned in section 5.1). Linier plot of Adams-Bohart model is shown in Fig. 5.7.

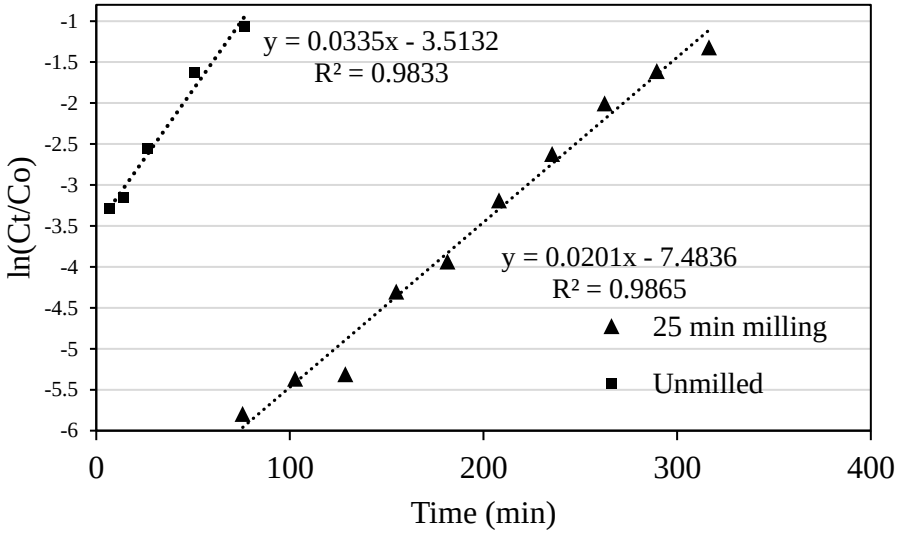

Fig. 5. 7 Linear plot of Adams-Bohart model

The Yoon-Nelson equation is given in eq. 1.9 and can be linearized as follows (eq. (5.9)):

$$\ln\left[\frac{C_t}{C_0 - C_t}\right] = k_{YN}t - \tau k_{YN} \tag{5.7}$$

where k_{YN} = the Yoon–Nelson rate constant (L/min), τ = the time in required for 50% sorbate breakthrough (min) (the values mentioned in section 5.1). Linear plot of Yoon-Nelson model can be seen in Fig. 5.8.

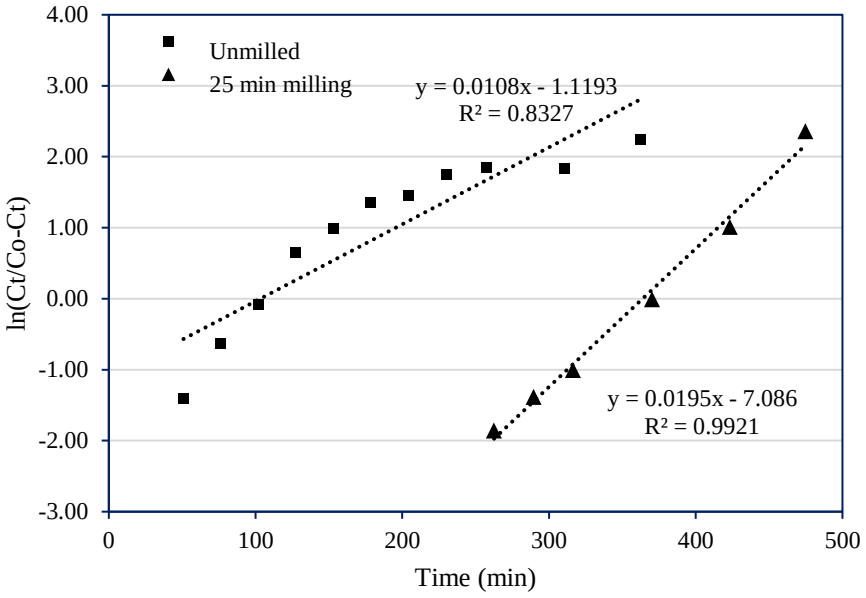

Fig. 5. 8 Linear plot of Yoon-Nelson model

Table 5.2, respectively presents the result calculations of Thomas, Adams-Bohart, and Yoon-Nelson models parameters obtained from slopes and intercepts of linear plots. The mathematical model and experimental breakthrough curves of unmilled and 25 minutes milled INB are given in Fig. 5.9.

Figure 5.9 shows Thomas and Yoon-Nelson models fit the experimental data, while Adams-Bohart model fit until initial breakthrough curve as it designed for practical until the initial breakthrough time. The R^2 shows all models fit which indicated closer to

1 for the milled INB, while for the unmilled Thomas and Yoon-Nelson does not show good linearization.

Table 5.2 Parameter of Thomas, Adams-Bohart, and Yoon-Nelson models for Mn sorption by INB in fixed-bed column before and after 25 minutes milling

Sample	Thomas model			Adams-Bohart model			Yoon-Nelson model		
	K_{Th} (L/min.mg)	q_0 (mg/g)	R^2	K_{AB} (L/min.mg)	N_0 (mg/L)	R^2	K_{YN} (L/min)	τ (min)	R^2
Unmilled	$4.6x10^{-4}$	3.91	0.83	0.0014	3284.2	0.98	0.01	103.64	0.83
Milled	$8.3x10^{-4}$	13.72	0.99	0.0009	11660	0.99	0.02	363.38	0.99

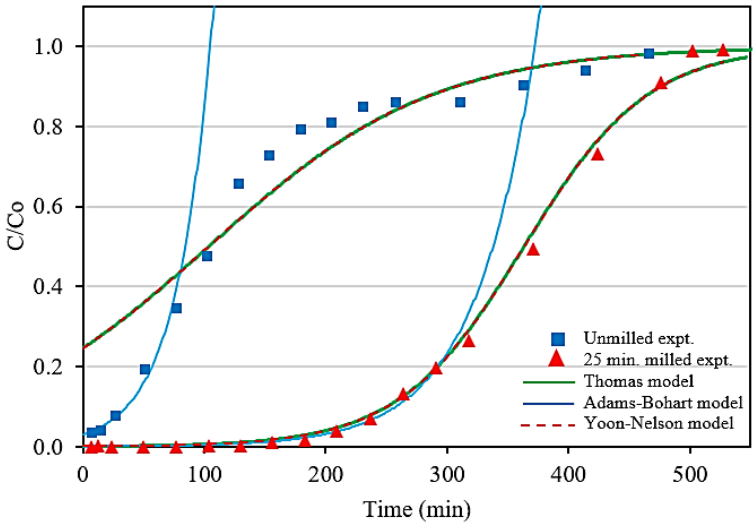

Fig. 5. 9 Comparison of the experimental and mathematical model breakthrough curves of Mn before and after milling modification of INB according to Thomas, Adams-Bohart, and Yoon-Nelson models.

5.3 Discussion

The breakthrough curves of milled INB in dynamic sorption study shows longer service time than the unmilled, indicates higher sorption capacity after ball-milling modification. The *MTZ* also became shorter after milling modification which is shown by

steeper breakthrough curve slope. Consequently, the *LUB* also shows far shorter after milling, indicates the bed becomes more efficient. The steeper breakthrough curve corresponds to faster sorption rate [4].

The coefficient of linear regression (R^2) in Table 5.2 shows Adams-Bohart model is more suitable and fit than Adams-Bohart model for both unmilled and milled INB. The Adams-Bohart showed always fitted because this model designed for practical purpose until the initial breakthrough time. After 25 minutes milling the R^2 of Thomas and Yoon-Nelson shows an increase until near 1 than the unmilled. This indicates the surface of INB before milling more heterogenic and becomes more homogenous after milling.

Breakthrough curves of milled INB in Fig. 5.9 also show a good agreement between the experimental and mathematical model of Thomas and Yoon-Nelson for the milled INB. The Thomas model, which parameter q_0 calculated the maximum Mn sorbed on the bed has an almost same result with the experimental calculation (q) (Table 5.1 and Table 5.2). This indicates the Thomas model was suitable for describing Mn sorption on milling modified INB where the external and internal diffusions are not the limiting step [5]. The Yoon-Nelson model is analogous to the Thomas model. The time required for 50% of sorbate breakthrough (τ) (Table 5.2) shows only slight different from the experimental after milling (370 min at C/C_0=0.5). Hence, besides the predicted breakthrough curves this parameter also proves a good agreement between experimental and Yoon-Nelson predicted model.

Another interesting finding in this dynamic sorption study is the breakthrough curves show asymmetrical curve before milling with indicated non ideal shape [6], and the asymmetric tent to decrease after 25 minutes milling on INB which means the curve after milling is closer to ideal (asymmetrical correspondent to the C/C_0=0.5 on breakthrough curves).

5.4 Summary

This chapter has presented some important points as follows:

- A significant change of breakthrough parameters after 25 minutes milling on INB: longer service time, shorter *MTZ* and *LUB*.
- The decrease in asymmetric breakthrough curve after 25 minutes milling.
- Mathematical model until equilibrium time suited to the Thomas and Yoon-Nelson model, while for the Adams-Bohart model only suited until initial breakthrough time. All the models showed improvement after milling modification, indicated by the values closer to 1 of R^2, almost similar value between experimental and model of Mn uptake and the time required for 50% of sorbate breakthrough, and more fitted predicted breakthrough curves.

References

[1] Herniwanti, J.B. Priatmadi, B. Yanuwiadi, Soemarno, Characteristics of acid mine water, Int. J. ChemTech Res. 6 (2014) 967–972.

[2] Indonesian Ministry of Life Environment, Standard quality for coal mining waste water, Indonesia, 2003. doi:10.1017/CBO9781107415324.004.

[3] C.J. Geankoplis, Transport Processes and Unit Operations, Prentice-Hall International, Inc., 1993.

[4] R. Eschrich, C.R.J. Guderian, M. Lange, Dynamic and equilibrium-based investigations of CO2-removal from CH4-rich gas mixtures on microporous adsorbents, Adsorption. 23 (2017) 197–209. doi:10.1007/s10450-016-9821-x.

[5] X. Lin, R. Li, Q. Wen, J. Wu, J. Fan, X. Jin, W. Qian, D. Liu, Experimental and Modeling Studies on the Sorption Breakthrough Behaviors of Butanol from Aqueous Solution in a Fixed-bed of KA-I Resin, Biotechnol. Bioprocess Eng. 233 (2013) 223–233. doi:10.1007/s12257-012-0549-5.

[6] R.L. Rodríguez, L. Candela, Transport of Cr(VI), Ni(II) and Mn(II) through metallurgical wastes. Batch and column experiments, in: React. Transp. Soil Groundw., Springer Verlag, 2005.

CHAPTER 6
Conclusions and recommendations

6.1 Conclusions

Overall, this research has achieved the following:

- Optimization ball-milling modification on INB for Mn removal from AMD has successfully reached the highest sorption capacity and pH improvement.
- The highest sorption capacity was achieved due to the loss of all cations in the octahedral sheet at 25 minutes milling that affected the maximum increase of negative surface charge of montmorillonite showed by the peak value of CEC. Continuous milling after this phase caused the sorption capacity started to decrease due to further amorphization in the tetrahedral sheet.
- The application of effective ball-milled INB on column sorbent has successfully given better performance than the unmilled showed by the maximum Mn sorbed, longer service time, and shorter *LUB*.

6.2 Recommendations

The improved result of INB in this study, however, is still the first step for real scale application since this bentonite has low hydraulic conductivity that will affect a long-time seepage in the outlet. Therefore, in order to increase the hydraulic conductivity, it is recommended to compose the milling modified INB with other materials such as sand, and also to conduct the column sorption test in large scale in further study.

Geostatistical investigation of bentonite potential in Wonosegoro is also recommended since the characteristics are not uniform. One sample conducted in this study only represent single geological outcrop in Garangan area which is a small part in Wonosegoro sub-district. Hence, to achieve successful utilization of Indonesian natural

bentonite in the whole Wonosegoro area for bed sorbent, cross-discipline study (i.e., chemical engineering, geostatistics, soil mechanic, and environmental engineering) are highly recommended and required.